Earth-Science Reviews 250 (2024) 104692

Contents lists available at ScienceDirect

Earth-Science Reviews

journal homepage: www.elsevier.com/locate/earscirev

Backwater length estimates in modern and ancient fluvio-deltaic settings: Review and proposal of standardized workflows

A.E. van Yperen [a,*], J.M. Holbrook [b], M. Poyatos-Moré [c], I. Midtkandal [a]

[a] University of Oslo, Department of Geosciences, P.O. Box 1047 Blindern, 0316 Oslo, Norway
[b] Texas Christian University, Department of Geological Sciences, TCU Box 298830, Fort Worth, TX 76129, United States of America
[c] Universitat Autònoma de Barcelona, Department of Geology, Edifici C, 08193 Bellaterra, Cerdanyola del Vallès, Spain

ARTICLE INFO

Keywords:
Backwater effect
Backwater length
Source to sink
Fluvio-deltaic strata
Modern river systems

ABSTRACT

The backwater effect (i.e. adjustments in open-channel flow as a response to proximity of standing water) is used to predict down-dip changes in morphodynamics and consequent sediment distribution on fluvial systems. However, there is currently no standardized method to obtain input parameters to estimate backwater length, nor where to measure these variables, for both modern and ancient settings. This study reviews existing methods for estimating backwater lengths in both settings and proposes workflows to minimize ambiguity in the results.

The proposed workflows are prioritized based on practicality, accuracy, and smallest uncertainty ranges and allow different data types as input parameters. For the first time, applying multiple methods to obtain backwater length estimates is tested, both on a modern and ancient river system. In the modern case study, the riverbed intersection with sea level matches previously documented major changes in sedimentary trends. However, backwater lengths based on h/S (h = bankfull thalweg channel depth, S = slope) plot downstream of this zone which is characterized by major changes, when input parameters are derived from discharge and grain size. Therefore, we recommend obtaining bankfull thalweg channel depth from a cross-sectional profile if backwater length is estimated based on h/S. In the ancient case study, bankfull thalweg channel depth derived from fully preserved single-story channel fill and slope based on Shields' empirical relation with grain size, match changes in fluvial architectural style interpreted as a result of backwater effects.

This review is a critical step forward in discussing and acknowledging the uncertainties and ambiguity in obtaining the necessary input parameters to estimate and compare modern and stratigraphic backwater lengths. The proposed workflows facilitate comparability and applicability of future backwater length estimates and subsequent interpretations of the hydrodynamic environment and resulting stratigraphic record. Potential scaling relationships between the backwater length, sedimentary trends, and avulsion nodes make this of key importance as the latter two also play a crucial role in devastating floods when rivers change course.

1. Introduction

Adjustments in open-channel flow as a response to the downstream proximity of a body of standing water are called 'backwater effects' and represent a change from normal to non-uniform flow conditions (Paola and Mohrig, 1996). Such effects are linked to sediment transport dynamics and resulting sedimentary architecture in the backwater zone, i.e. the reach of the riverbed profile over which non-uniform flow conditions occur (Lamb et al., 2012; Nittrouer et al., 2012; Chatanantavet et al., 2012; Blum et al., 2013; Chatanantavet and Lamb, 2014; Colombera et al., 2016; Fernandes et al., 2016; Martin et al., 2018; Trower et al., 2018; Ganti et al., 2019; Gugliotta and Saito, 2019; Wu et al., 2023).

The streamwise distance over which adjustments in flow dynamics occur is governed by the length scale h/S (where h is channel depth and S is slope) and was termed 'backwater length' by Paola and Mohrig (1996). This length scale is derived from basic fluid momentum balances in which the Froude number is a critical parameter determining whether or not downstream boundary conditions such as base level can influence upstream hydrodynamics (Paola and Mohrig, 1996):

$$F^2\left[\frac{H^2 2g}{L}\right] \sim \left[\frac{H^2 g}{L}\right] + HgS + \frac{\tau}{\rho} \quad (1)$$

* Corresponding author.
E-mail address: a.v.yperen@geo.uio.no (A.E. van Yperen).

https://doi.org/10.1016/j.earscirev.2024.104692
Received 18 April 2023; Received in revised form 19 December 2023; Accepted 18 January 2024
Available online 24 January 2024

Where H is depth, τ is Shear stress, F is the Froude number, g is gravitational acceleration, S is slope, L is streamwise length scale and ρ is density. The width of the zone where the Froude number ≪ 1 and the water surface slope ≪ bed slope, is the backwater length (Paola and Mohrig, 1996; Hajek and Wolinsky, 2012). This equation applies to open-channel dynamics and disregards basinal processes such as tides and waves. Backwater *lengths* can be estimated and are applicable despite the dominant process regime but the exact impact of tide- or

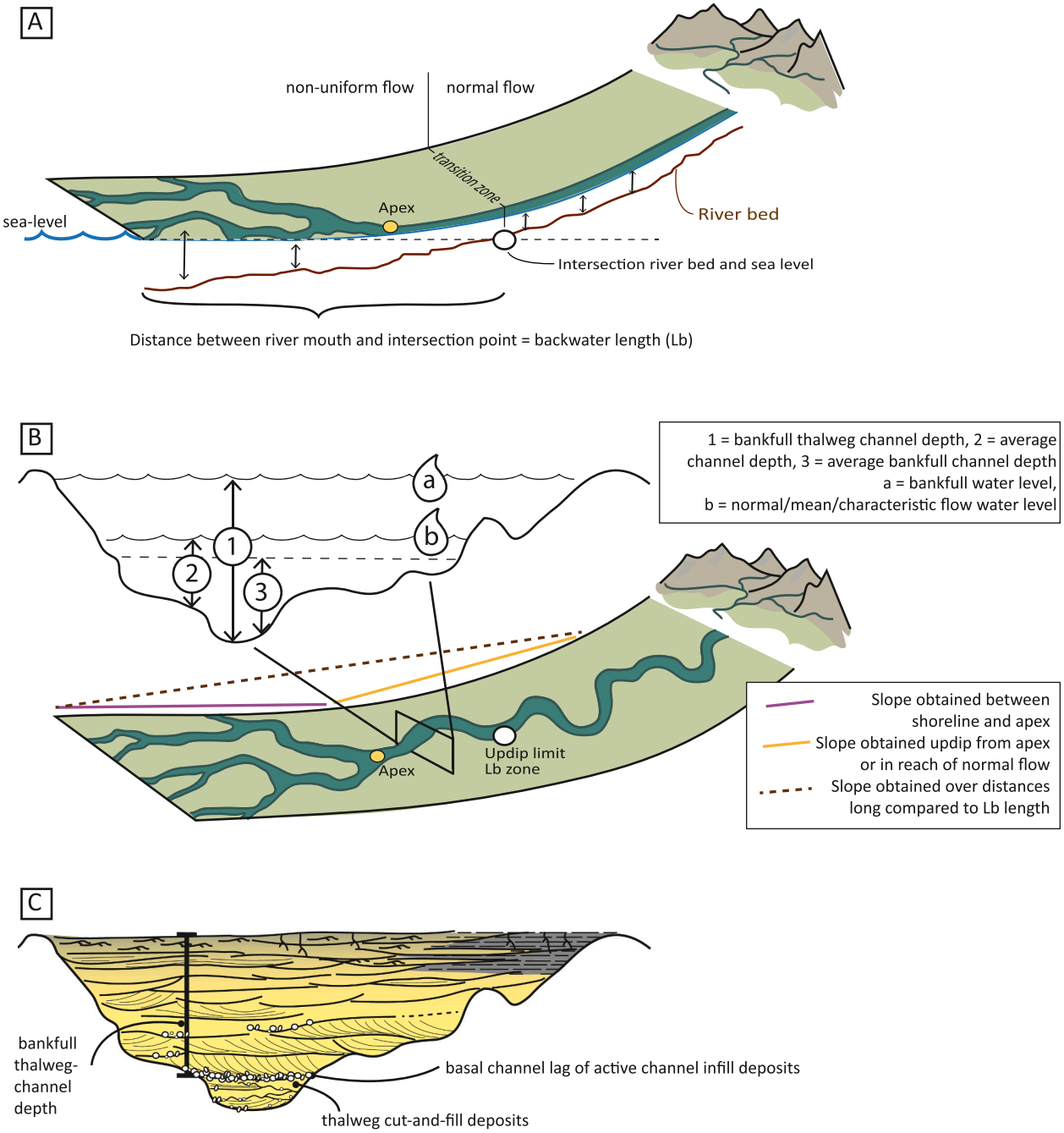

Fig. 1. (A) Backwater length is the streamwise distance over which adjustments in flow dynamics occur as a response to approaching a standing body of water (Paola and Mohrig, 1996). This matches the intersection between riverbed and sea level (Nittrouer et al., 2011; Blum et al., 2013; Fernandes et al., 2016; Smith et al., 2020). (B) Summary of differences in current acquisition methods for backwater length estimates. In cross-sectional view: ambiguity arises from differences in used water level: a) bankfull water level or b) normal/mean/characteristic flow level. Differences in type of channel depth enhance incomparability of backwater estimates; 1) bankfull thalweg channel depth, i.e. deepest point in the channel, at times of water level a, and 2) average channel depth, i.e. linked to water level b, or 3) average bankfull channel depth, which is obtained differently by different authors (see section 3.2). Along the down-dip transect, the colored lines represent slopes measured over different distances as used in publications addressing backwater estimates in modern river systems (Table 3). Such differences will result in different backwater length estimates. (C) When measuring bankfull thalweg channel thickness in ancient settings, basal thalweg fill deposits should be excluded. See section 2.3.

wave-influenced backwater hydrodynamics on morpho-sedimentary channel characteristics will have to be assessed by future work (Gugliotta and Saito, 2019). Therefore, the backwater effect is currently considered best applied to single-thread systems on river-dominated delta plains (Hartley et al., 2016).

The change from normal to non-uniform flow conditions matches the bankfull *thalweg* channel bed intersecting with sea level and several changes in sedimentary patterns (Wright and Parker, 2005; Nittrouer et al., 2011; Blum et al., 2013; Nittrouer, 2013; Fernandes et al., 2016) (Fig. 1A). Field surveys for the lower Trinity River in east Texas (USA) show that where the riverbed elevation drops below sea level, the low-flow water depth gradually increases and matches large-scale changes in geomorphology (Smith et al., 2020). Blum et al. (2013) and Fernandes et al. (2016) specifically mention that the backwater length corresponds to the distance over which the scoured channel base is at or below sea level. Strong relationships between this backwater length scale and sedimentary trends are dominantly derived from studies on the Mississippi river (Hudson and Kesel, 2000; Nittrouer et al., 2011, 2012; Blum et al., 2013; Nittrouer, 2013) and more scarcely the Trinity river (Smith et al., 2020), and Rhine river (Fernandes et al., 2016).

In modern river systems, the backwater length (Lb) is determined using direct field measurements of bankfull thalweg channel depth and its intersection with sea level (Nittrouer et al., 2011; Gugliotta et al., 2017; Smith et al., 2020). Alternatively it can be estimated indirectly by Lb = h/S, where h is bankfull channel depth along some consistent thalweg profile that excludes localized scour holes, and S is channel slope (Jerolmack, 2009; Chatanantavet et al., 2012; Blum et al., 2013; Ganti et al., 2014, 2016; Hartley et al., 2016; Fernandes et al., 2016; Brooke et al., 2020, 2021; Prasojo et al., 2021). This equation is also used to estimate backwater length in ancient settings (Colombera et al., 2016; Lin and Bhattacharya, 2017; Kimmerle and Bhattacharya, 2018; Martin et al., 2018; Trower et al., 2018; Lin et al., 2020; van Yperen et al., 2021; Wu et al., 2023). However, there is currently no standardized method to measure slope and channel depth, nor consensus on where to measure these variables, for both modern and ancient settings (Fig. 1B). This is illustrated by different backwater length estimates for the same modern river resulting from different methods that vary up to a factor 10 (Fig. 2, Table 1). Additionally, in both modern and ancient settings, ambiguity arises from the use of different water levels and whether to use maximum / thalweg bankfull or average channel depth (Fig. 1), which consequently impacts resultant backwater length estimates.

The aims of this paper are: 1) to compile previously applied methods for estimating backwater lengths in modern and ancient settings and provide an overview of their differences, sources of error, and limitations, 2) to discuss challenges and limitations of collecting input parameters, 3) to propose workflows based on available input data and unified methods to estimate backwater lengths in both modern and ancient settings, aiming to minimize ambiguity and maximize practicality, 4) to test the proposed workflows on both a rock record and modern-river case study, and 5) to discuss uncertainty factors for each workflow, as well as the shortcomings, applications and recommendations of using the backwater concept generally.

2. Backwater length estimates in ancient settings

A range of prior works offer a spectrum of methods for determining paleohydraulic parameters applicable to ancient fluvial strata and attempt to update these equations using empirical re-evaluation of modern stream data (e.g., Holbrook and Wanas, 2014; Long, 2021; Lyster et al., 2023). Here we focus specifically on publications estimating backwater length and related methods to obtain input values for

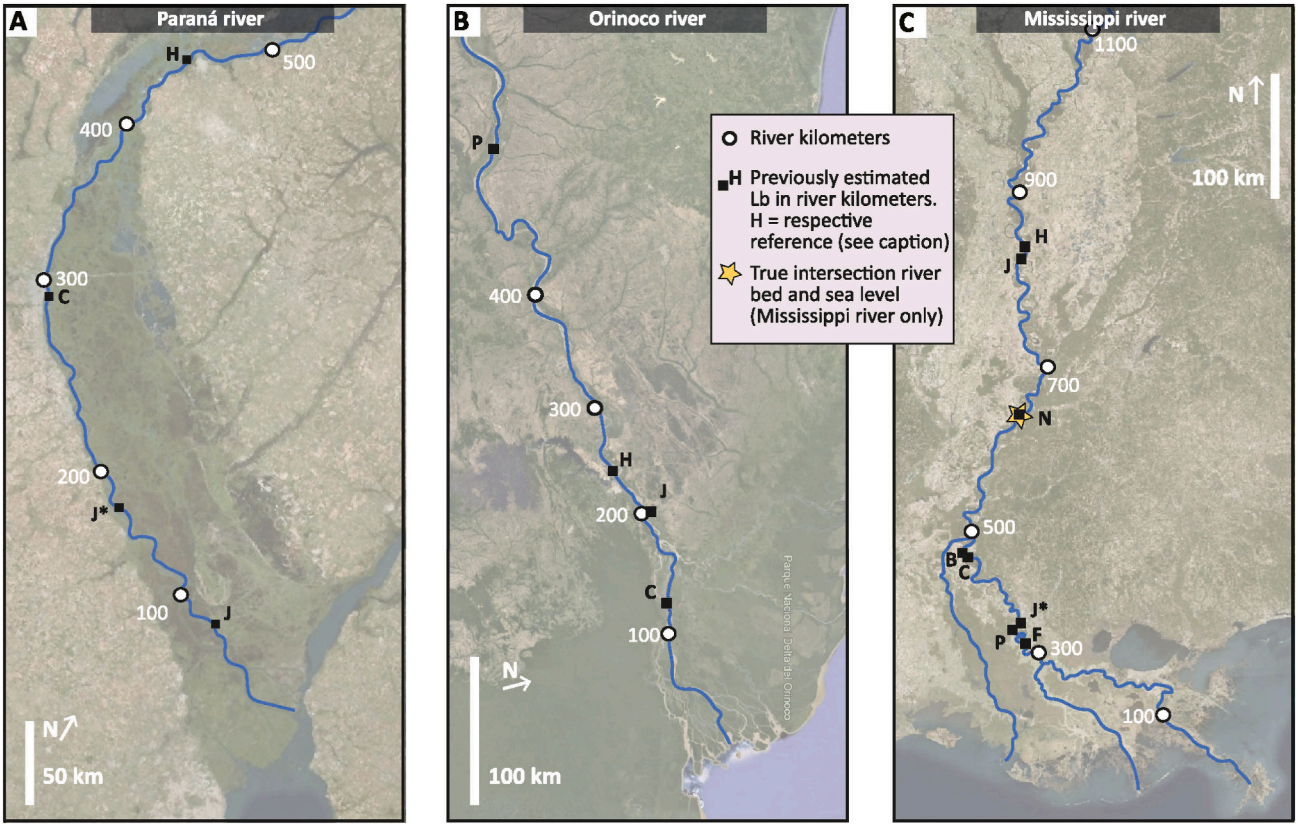

Fig. 2. Backwater length estimates based on Lb = h/S and displayed in river km by different authors for the Paraná River (A), Orinoco (B), and Mississippi River (C). J = Table 1 in Jerolmack (2009), J* = Fig. 9 and 14 in Jerolmack (2009), B = Brooke et al. (2021), C = Chatanantavet et al. (2012); F = Fernandes et al. (2016); H = Hartley et al. (2016), P = Prasojo et al. (2021). See Table 1 for Lb estimates.

Table 1
Table listing modern deltas for which the Lb (km) has been estimated in multiple publications. See Fig. 2 for a map view of a selection of these deltas. Note: Lb lengths for the Mississippi River and Paraná River for Jerolmack (2009) are computed based on the values listed in Table 1 in Jerolmack (2009). However, Lb lengths for these rivers are displayed differently on the figures in the same publication. Note a factor 5 difference for Amazon Lb estimates, and more than a factor 10 for the Rhône and Danube rivers.

River	Country	Prasojo et al., 2021	Hartley et al., 2016	Jerolmack, 2009	Chatanantavet et al., 2012	Brooke et al., 2021	Nittrouer et al., 2011	Fernandes et al., 2016	Ganti et al., 2014	Gugliotta et al., 2017
Amazon	Brazil	–	1952	–	400	–	–	–	–	–
Brahmaputra	Bangladesh	–	278	70	–	–	–	–	–	–
Danube	Romania	1543	–	125	125	126	–	–	–	–
Ebro	Spain	19	–	30	–	–	–	–	–	–
Magdalena	Colombia	169	–	63	63	63	–	–	–	–
Manitoba	Canada	–	–	5	8	–	–	–	–	–
Mekong	Vietnam, Cambodia	692	–	–	–	–	–	–	–	560
Mississippi	USA	338	842	833	480	488	680	328	–	–
Niger	Nigeria	113	256	–	–	–	–	–	–	–
Nile	Egypt	92	340	120	254	253	–	–	–	–
Orinoco	Venezuela	586	240	200	133	133	–	–	–	–
Paraná	Argentina	–	451	73	295	295	–	–	–	–
Rhine-Meuse	Netherlands	–	–	45	46	45	–	71	–	–
Rhône	France	9	81	148	–	–	–	–	–	–
Volga	Russia	184	–	180	–	–	–	–	–	–
Zambezi	Mozambique	23	72	–	–	–	–	–	–	–
Huange / Yellow	China	–	25	10	–	41	–	–	21–54	–

slope and channel depth (Table 2).

2.1. Location to measure slope and channel depth

In ancient settings, slope and channel depth estimates are obtained from a few selected locations, which contrasts with studies from modern river systems, in which channel depth and slope measurements are commonly averaged over more comprehensive measurements along continuous river reaches (Fig. 1, Table 2).

Channel depth and slope are i) 'evaluated upstream in reach of normal flow' (Trower et al., 2018; van Yperen et al., 2021; Wu et al., 2023), ii) obtained in 'relatively proximal portions of the paleodelta system'(Kimmerle and Bhattacharya, 2018; Martin et al., 2018), iii) inferred from the gradient of back-stripped stratigraphic correlation across the full fluvial to marine-shelf profile or iv) lack further specification (Table 2). Paola and Mohrig (1996), a foundational paper of the backwater effect, note that 'the key point is that the depth, slope, and shear stress refer to conditions averaged over distances that are long compared with the backwater length' and that 'the idea is to approximate as closely as possible the measurement of an average depth over a section across a modern river'.

Recommendations: the location to measure slope and channel depth is inherently connected to the selected method to estimate these two parameters, and may depend on the available data (e.g. outcrop extent, coverage of subsurface data set). Slopes generally decrease towards the shoreline as the channel enters the backwater zone, which implies that backwater lengths calculated from slopes obtained within the backwater zone are longer than those calculated from slopes obtained up-dip of the backwater zone, for the same river. We recommend that paleohydraulic analysis should be calculated for normal-flow zone conditions, i.e. landward of the backwater zone (e.g. Fernandes et al., 2016), to allow comparison between normal flow parameters versus paleohydraulic estimates obtained in the backwater zone, and to evaluate backwater effects on sedimentation patterns. This implies a chicken-and-egg situation; one needs to select a location to derive depth and slope to estimate backwater length, but the length is needed to define the upstream limit of non-uniform flow condition, which in turn determines where to sample channel depth and slope. Alternatively, changes in fluvial architectural style could be used to interpret the presence/absence of backwater conditions (van Yperen et al., 2021), but this implies a causal relationship between the two, which is unwanted in cases where the effects of backwater processes on sedimentation patterns are to be tested. We therefore recommend an iterative process that narrows the potential backwater length by estimating values at multiple locations until the sample is upstream of a reasonable backwater estimate and therefore in normal-flow conditions.

2.2. Channel depth type

A variety of channel depth types are listed for estimating backwater lengths in ancient settings: bankfull channel depth, bankfull thalweg depth, average bankfull channel depth, characteristic channel depth, and characteristic bankfull flow depth (Fig. 1, Table 2). Only a few publications specify exactly what they mean with their selected channel depth type (Bridge and Tye, 2000; Leclair and Bridge, 2001; Holbrook and Wanas, 2014; Lin and Bhattacharya, 2017; Long, 2021). Moreover, these few cases highlight that usage of the same term does not imply the same understanding and hence application of the selected depth type: 'average bankfull channel depth' has been explained as i) one-half of the maximum bankfull thalweg depth (Bridge and Tye, 2000; Leclair and Bridge, 2001; Holbrook and Wanas, 2014); ii) the average of multiple maximal bankfull measurements (Lin and Bhattacharya, 2017); and iii) the average bankfull depth across a full cross-sectional profile (Long, 2021). Finally, the – unintended – mixing of terminology is illustrated by publications using the same method to establish channel depth, but using different terms for the channel depth *type* (cf. Martin et al., 2018; van Yperen et al., 2021; Table 2).

Recommendations: when deciding which channel depth type to use for backwater estimates, it is essential to 1) consider the hydrodynamic meaning of the different depth types, and 2) define what the recommended channel type implies, i.e. clarifying the terminology used to minimize ambiguity when discussing methods to obtain this parameter. Hydrodynamically, the backwater zone is a reach of changing morphodynamics, and therefore the channel type and -stage mostly affected by such changes should be used to obtain backwater length estimates. Adjustments in channel morphology are considered to occur predominantly at bankfull conditions (Williams, 1978) albeit that a range of discharges, rather than a single event magnitude, can determine the morphology and long-term stability of a given channel-reach (Pickup and Warner, 1976; Pickup and Rieger, 1979; Graf, 1988; Surian et al.,

Table 2
Overview of selected publications addressed in this review and their methods to obtain input parameters to estimate backwater length in ancient settings. Direct quotations in *italic*.

Reference	Study type	Slope measurement location	Slope measurement method	Channel depth	Depth measurement location	Depth measurement method
Colombera et al., 2016	Outcrop, Cretaceous Neslen Formation	No comments	Inferred from the gradient of transgressive surfaces	Bankfull depth	No comments	Maximum bar thickness or cross-strata set tickness
Lin and Bhattacharya, 2017	Outcrop, Cretaceous Dunvegan Alloformation	$\tau^*bf\ 50 = (dmS)/(PD50) =$ constant No comments	sensu Holbrook and Wanas (2014) and Trampush et al. (2014)	Bankfull channel depth	No comments	Channel-depth values estimated from multiple methods; fining-upward channel stories, point-bar deposits, lateral-accretion bars, average cross-set thickness, statistics from well-log data. Use of minimum and maximum average value of compiled channel depths.
Trower et al., 2018	Outcrop, Cretaceous Castlegate Sandstone	*"Evaluated upstream in reach of normal flow"*	Slopes were calculated using Shields relation: $\log S = -2{,}08 + (0{,}254*\log D_{50})-(1{,}09*\log H_{bf})$ sensu Trampush et al. (2014)	*"Characteristic bankfull flow depth"*	*"Evaluated upstream in reach of normal flow"*	Bankfull depth inferred from bar heights and scour depths measured in a transect along the paleo-flow direction.
Kimmerle and Bhattacharya, 2018	Outcrop, Cretaceous Ferron Sandstone	Stratigraphicallly derived slope and estimates based on Holbrook and Wanas (2014). D50 for each valley, within the backwater zone.	D_{50} and bankfull channel depth were used to estimate channel slope, as per the method described by Holbrook and Wanas (2014) and method 1 of Lynds et al. (2014). They also use slope estimates based on long-profile erosional relief of Ferron incised valleys (Zhu et al., 2012)	Bankfull channel depth	Within the backwater zone, interpreted to be at the landward end of the backwater zone.	Backwater in their table 5, paleohydraulics in their Table 2 and 3. Paleohydraulic analysis based on measured point-bar thickness and cross-set thickness (Bridge and Tye, 2000; Leclair and Bridge, 2001; Holbrook and Wanas, 2014) compared with estimates directly derived from outcrop exposures, by using rollover geometries in accreting-point-bar deposits as representative of complete bar preservation (Hajek and Heller, 2012)
Martin et al., 2018	Subsurface, Triassic Mungaroo Formation	*"Relatively proximal portions of the Mungaroo paleodelta system"*, acknowledging potential influence of non-uniform flow conditions	Using a global dataset that relates particle size (D) and boundary shear stress (τ) from modern rivers (Trampush et al., 2014): $S = \tau/(gH_{ch})$. Produced range of paleoslope estimates to include natural variability in bankfull shear stress.	Characteristic channel depth	*"Relatively proximal portions of the Mungaroo paleodelta system"*, acknowledging potential influence of non-uniform flow conditions	Dune height from cross-set thickness (Paola and Borgman, 1991) and flow depth from dune height (Yalin, 1964; Allen, 1983) and subsequent syntheses (Leclair and Bridge, 2001; Venditti, 2013).
Lin et al., 2020	Outcrop, Cretaceous Gallup Sandstone	Regional sequence stratigraphic correlation from fluvial to marine shelf, or fluvial section only. Grainsize samples from both fluvial and terminal distributary channel deposits.	Stratigraphic correlations and numerically; $\tau^*_{bf50} = (d_mS)/(PD_{50})$	Bankfull flow depth	From a fluvial channel and two terminal distributary channel deposits.	Bankfull flow depth btained from fully preserved channel stories or from dune-scale cross bedding and bar accretion deposits, using 6-10× average dune height to calculate average channel depth, and dune heigh is 2.9 (± 0.7) x the average cross-set thickness (Leclair and Bridge, 2001)
van Yperen et al., 2021	Outcrop, Cretaceous Dakota Group	*"Evaluated upstream in reach of normal flow"*	$\tau^*bf\ 50 = (dmS)/(PD50)$	Bankfull flow depth	*"Evaluated upstream in reach of normal flow"*	Bankfull channel depth inferred from completely preserved trunk channel deposits or mean dune height calculated from cross-set thickness (Leclair and Bridge, 2001) from which bankfull paleoflow depths are calculated (Allen, 1982; Best and Fielding, 2019; Bradley and Venditti, 2017)
Wu et al., 2023	Outcrop, Carboniferous Tully Sandstone	$\tau^*bf\ 50 = (dmS)/(PD50) =$ constant In normal flow conditions	sensu Lynds and Holbrook, log S = -2,08 + (0,254*logD50)-(1,09*logHbf) sensu Trampush et al. (2014), and stratigraphic inversion	Flow depth	In normal flow conditions	Stratigraphic restoration, and dune height calculated from cross-set thickness (Leclair and Bridge, 2001) from which flow depth is calculated using the scaling relationship from Bradley and Venditti (2017)

2009). Therefore, we consider 'bankfull channel depth' as the defining stage to assess changes in channel morphology caused by backwater effects. Using either maximum or average bankfull channel depth may significantly impact resulting backwater length estimates, as maximum channel depths can locally be up to five times average flow depth (Bridge and Mackey, 1993; Best and Ashworth, 1997). Hydrodynamically, the deepest part of a channel cross-section is considered an important formative factor as its area is important for determining the possible maximum discharge flux. In practical terms, bankfull channel thalweg depth can be directly measured in outcrop, core, and well-log studies; based on preserved single-story thickness, provided that such fining upward channel successions are fully penetrated or exposed and not significantly truncated at their top (Bridge and Tye, 2000; Hajek and Heller, 2012; Holbrook and Wanas, 2014; Milliken et al., 2018; Long, 2021). However, some error is still introduced as thalweg depth can vary along the channel bottom and this approach is a proxy for thalweg depth in one specific channel cross section. Additionally, complete vs partial channel-fill sections can be challenging to distinguish in boreholes where no lateral context is available. Finally, for the reasons listed above, applying any type of 'average' channel depth to backwater calculations in the ancient, as opposed to thalweg depth, is a recipe for confusion as there are different understandings of how to achieve the average value (cf. Bridge and Tye, 2000; Leclair and Bridge, 2001; Holbrook and Wanas, 2014; Lin and Bhattacharya, 2017; Long, 2021).

Taking all the above into consideration, we recommend using bankfull thalweg channel depth, i.e. the maximum depth across a cross-sectional channel profile related to bankfull flow conditions (Fig. 1, see section 5.2), as this represents bankfull flow conditions which are considered to represent channel forming conditions. Additionally, bankfull thalweg depth is more easily obtained from outcrop, and the term itself minimizes ambiguity as max*imum* depth is unambiguous and therefore pragmatic and consistent.

2.3. Methods to obtain bankfull thalweg channel depth

Methods used to infer channel depth for backwater length estimates in ancient settings are twofold: i) direct measurements in the field, such as from maximum scour depth or maximum bar thickness, and ii) empirically by estimating flow depth from dune height from mean cross-set thickness (Table 2). Stratigraphic restoration is only used by Wu et al. (2023). Notably, none of the publications in Table 2 factors in decompactions.

Recommendations: A correction for burial compaction should be performed where compaction is expected, either after acquiring mean cross-set thicknesses used for empirically estimating channel depth or onto thicknesses derived from direct field measurements of preserved single-story channel deposits. Ideally, the decompaction factor should be estimated based on thin-section data. If not available, a decompaction factor of 1.1 is commonly used for sandy bar stories (Holbrook and Wanas, 2014; Long, 2021), although the likely range is between 1.0 and 1.69 for channel stories in general (Long, 2021).

We recommend inferring bankfull thalweg channel depth from completely preserved single-story trunk channel deposits, if data availability allows, as this provides smaller uncertainty ranges than bankfull thalweg channel depth inferred empirically from average cross-set thickness (see section 4). When estimating channel depth from reconstructed dune heights, the use of fully preserved single-story channel thicknesses as a calibration is a useful approach (Hartley and Owen, 2022). Other channel elements often used to obtain channel depth from direct outcrop measurements, such as barforms and large-scale planar cross-strata, typically represent less than bankfull thalweg depth (Bridge, 2003; Bhattacharya et al., 2016). Note that channel belt thickness often includes basal thalweg fill deposits. These tend to record short-term and iterative bypass and erosion phases resulting from ephemeral and/or local cut-and-fill events or are aggradational belt strata predating the infill of the active channel (Mclaurin and Steel, 2007; Holbrook and Wanas, 2014). These are not part of the active channel-fill story thickness, add additional thickness that is not representative of more typical bankfull thalweg flow conditions, and should be excluded from estimates of bankfull channel depth (Holbrook and Wanas, 2014) (Fig. 1C). Finally, it is important to avoid very localized deep holes or particularly shallow riffles.

When estimating flow depth empirically, from dune height via mean cross-set thickness, we recommend using the relation of Leclair and Bridge (2001) to infer mean dune height, h_d, from mean cross-set height, $h_{xs\text{-}mean}$:

$$h_d = 2.9(\pm 0.7)h_{xs-mean} \quad (2)$$

Cross-set thicknesses should be measured on trough and/or tabular cross-bedding, as these are sedimentary structures from bedforms indicative of bedload transport (Rubin and Carter, 1987). A newly established relationship between maximum ($h_{xs\text{-}max}$) and mean cross-set height ($h_{xs\text{-}mean} = 0.7(\pm 0.01)h_{xs\text{-}max}$) allows collection of maximum cross-set thickness in the field rather than height distributions of individual cross-sets (Fig. 5A *in* Lyster et al., 2021). Maximum cross-set measurements should be collected from the lowermost bedforms, as these are representative of formative flow depth.

To scale mean dune height (h_d) to formative flow depth (H), we recommend using Bradley and Venditti's (2017) scaling relationship, based on 382 field observations, where:

$$H = 6.7h_d \quad (3)$$

Note this scaling relationship represents a conversion to *average* depth rather than *thalweg* channel depth, and therefore an additional conversion of some multiple is needed to adjust this value to a representative thalweg depth. Typically applied multipliers for a conversion from average to bankfull thalweg channel depth are 1.44 (Long, 2021, modified from Bjerklie et al., 2018), ~1.7 (Bridge and Mackey, 1993), and 2 (Leclair and Bridge, 2001). Variations among these scaling relationships reflect differences in channel type and thereby its cross-sectional shape. For instance, highly asymmetrical channels (e.g., highly sinuous meander bends) exhibit significantly different average-to-thalweg channel depth ratios compared to symmetrical channels (e.g., cross sections at meander crossovers or in braided rivers), where average channel depth can be close to thalweg channel depth. Where additional data are available (e.g., seismic data, etc.) that help constrain river patterns and/or cross section position, we recommend selecting an 'educated conversion' from average to thalweg channel depth adjusted to channel style to improve accuracy (Fig. 3).

2.4. Methods to obtain slope

Methods used to obtain slope for backwater length estimates in ancient settings are two-fold: i) empirically, based on its relation to grain size and ii) based on stratigraphic correlations (Table 2). Kimmerle and Bhattacharya (2018) and Lin et al. (2020) use both these methods and show that empirically derived slopes are approximately five to ten times smaller than stratigraphically derived slope estimates, significantly impacting backwater length estimates. The empirically derived slopes are based on the relationship between grain size and Shields stress:

$$S = RD_{50}\tau^*/H \quad (4)$$

where S is the slope, R is the dimensionless submerged specific gravity of sediment in water with 1.65 for quartz, τ^* is the Shields number for dimensionless shear stress, and H is the flow depth (Shields, 1936; Parker, 1978; Holbrook and Wanas, 2014; Lynds et al., 2014; Trampush et al., 2014). An important note is that this method is based on *average* bankfull flow depth, and not bankfull *thalweg* flow depth (Holbrook and Wanas, 2014). Therefore, if bankfull thalweg depth is used (e.g. fully preserved channel story thickness measured on an outcrop) a conversion to average bankfull flow depth will need to be made before using this

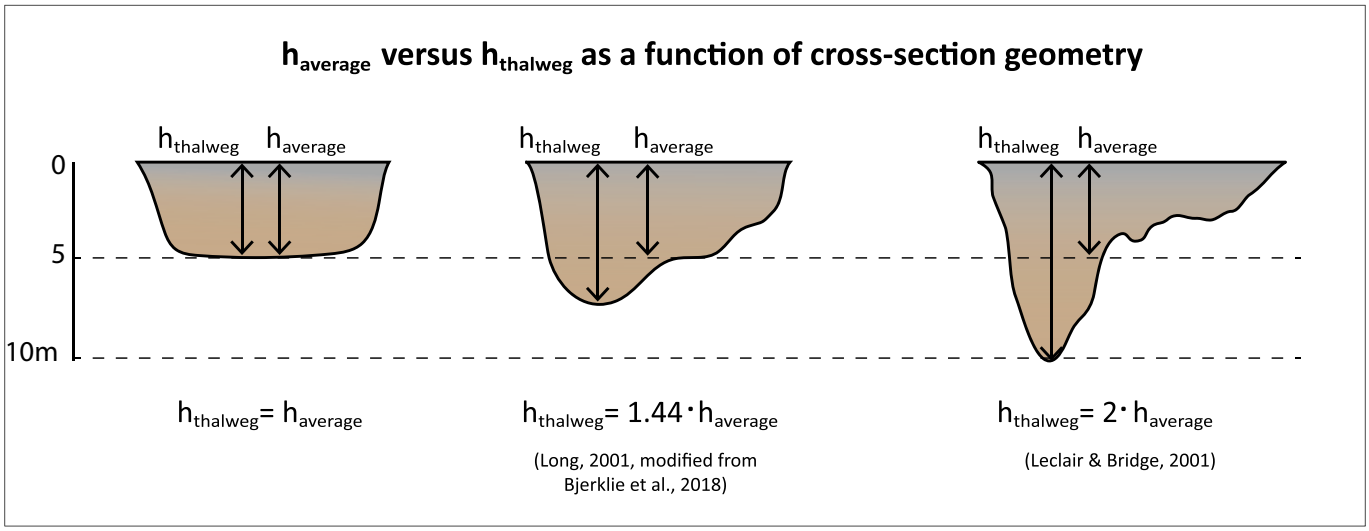

Fig. 3. A most accurate multiplier to convert average ($h_{average}$) to thalweg channel depth ($h_{thalweg}$) depends on the cross-sectional channel shape.

equation.

It is worth noting that slope estimates based on eq. 4 may be up to a factor 2 greater than those based on eq. 5:

$$\mathrm{LogS} = \alpha_0 + \alpha_1 \mathrm{logD50} + \alpha_2 \mathrm{logH} \quad (5)$$

where H is bankfull channel depth and the constants are given by $\alpha_0 = -2.08 \pm 0.036$, $\alpha_1 = 0.254 \pm 0.016$, and $\alpha_0 = -1.09 \pm 0.044$ (Trampush et al., 2014; Lyster et al., 2021).

Recommendations: In general, there is yet no clear path to resolve river gradients in ancient deposits, as variables such as sinuosity, climate, and grain size all play a significant role and uncertainty in inputs many may introduce potential errors, regardless of the method used (Long, 2021). It is beyond the purpose of this paper to provide a full review of methods to estimate slope.

According to Long (2021), empirical relationships for slope estimates with eq. 4 generally plot lower than the observed slope, and therefore he recommends using a different relationship (i.e. $S = 0.0239\ (D_{50}/d_{bf})^{0.4763}$). However, we propose to use eq. 4 regardless, because: i) the relationship proposed by Long (2021) has an uncertainty factor of 27 (see Supplemental Text S4) whereas eq. 4 has an uncertainty factor of 2 (Holbrook and Wanas, 2014), ii) most streams have more competence than is reflected by the grain-size supply (e.g. Paola et al., 1992), which explains the underestimation of slopes based on eq. 4 (Shields stress), iii) both equations require similar data collection efforts as they both utilize grain size samples as an input parameter.

Sampling from an interval representative of bedload transport at times of formative (bankfull) discharge is implicitly required in slope calculations based on grain size. We recommend avoiding samples from thalweg deposits or lags at the channel base as they might not represent the most common bedload transport conditions, and instead sampling from the lowest representative bedform in a given story (Holbrook and Wanas, 2014). Bedforms positioned higher within the individual channel deposit are best avoided as they are more likely to record infill processes which are under-representations of the formative flow conditions. Additionally, for grain size analysis we recommend using a laser particle size analyzer after rock sample disaggregation rather than thin section analysis where samples can be disaggregated without significant grain breakage or retention of cement coatings, as the first measures silt and clay portions more accurately (Brooks et al., 2022).

If grain size is not available, slope can be based on bankfull channel width (w_{bf}) using Long (2021):

$$S = 0.0341 \times w_{bf}^{-0.7430} \quad (6)$$

where W_{bf} is bankfull channel depth. Bankfull channel width can be directly measured from outcrop albeit channel widths should be corrected for outcropping cut oblique to cross-stream direction.

3. Backwater length estimates in modern river systems

Existing backwater estimate methods in modern river systems are compiled from fourteen publications (Table 3) and are twofold; i) direct assessments of the intersection between riverbed and sea level, and ii) indirect estimate by obtaining input parameters river depth and slope and applying $L_b = h/S$ with L_b is backwater length, h is river depth, and S is slope. Backwater effects are also studied in engineering (Csiki and Rhoads, 2010; Maselli et al., 2018; Liro, 2019; Liro et al., 2020; Amarnath and Thatikonda, 2020), The backwater zone is the river section upstream of a dam reservoir, submerged when reservoir levels exceed the normal or average stages. (Liro, 2019), characterized by backwater and drawdown surface water profiles associated with varying low-discharge and high-discharge events (Maselli et al., 2018). In this study, and particularly this section, we focus on backwater length estimates in coastal river systems unrelated to river dams.

3.1. Location to measure slope and channel depth

In modern rivers, slope and channel depth measurements are often averaged over a certain river section for backwater length estimates (Fig. 1, Table 3). Slope estimates are obtained along inconsistent river segments; i) in normal flow reaches, ii) across 25 km upstream of the avulsion site, iii) 'upstream of the delta', iv) 'between the bankfull elevation at the delta apex and the shoreline', v) as a continuous profile over distances longer than the backwater length or vi) lacking further specification (Fig. 4C, Table 3). Both Jerolmack (2009) and Hartley et al. (2016) list backwater length for the same set of deltas, in which estimates by Hartley et al. (2016) are consistently longer than those by (Jerolmack, 2009) (Table 1, Fig. 2). Their different choices for the location to obtain river slope partly explains this discrepancy; delta plain slopes (c.f. Hartley et al., 2016) tend to be lower than river slopes upstream of the apex (c.f. Jerolmack, 2009), in addition to channel depths listed by Hartley et al. (2016) being thicker (Table S1 and S2). Because river surface elevation profiles asymptotically approach the relatively fixed water surface elevation of the receiving basin (Chow, 1959), obtaining slope from different segments results in different steepness which may lead to backwater lengths with up to a factor 2 difference, based on results from the Mississippi river (Fig. 4A, Table S3A).

Table 3
Overview of selected publications addressed in this review and their methods to obtain input parameters to estimate backwater length in modern river systems. Direct quotations in italic.

Reference	Study type	Slope measurement location	Slope measurement method	Channel depth type	Channel depth measurement location	Depth measurement method
Paola and Mohrig, 1996	Ancient & modern rivers	*"depth, slope and shear stress refer to conditions averaged over distances that are long compared with backwater length"*	Determine average and median values for depth and grainsize. Subsequently calculate a single slope estimate.	Channel depth	*"depth, slope and shear stress refer to conditions averaged over distances that are long compared with backwater length"*	*"… measuring as many depth indicators as possible over the oucrope area."*
Jerolmack, 2009	Mathematical model and the Mississippi and Rhine-Muse rivers	*"S is the river slope upstream of the delta"*	*"Hydraulic and geometric parameters, compiled from literature"*	Channel depth. No specification, but their Fig. 7 suggests it might be bankfull	No comments	No comments - their Fig. 8 indicates channel depth from Jerolmack and Mohrig (2007). We cannot retrieve depth from Jerolmack and Mohrig (2007).
Nittrouer et al., 2011	Mississippi river	Slope is measured for the lower 1050 river kilometers.	Slope is measured from low, moderate and high water level surface elevation at 18 gauge stations.	Thalweg depth	Lower 1050 river kilometers	Hydrographic river bed survey (from Harmar and Clifford, 2007).
Chatanantavet et al., 2012	2D model and 9 modern river deltas	No comments about location.	*"The channel slope for each river was calculated from existing literature"*	Characteristic flow depth = normal flow depth	*"Upstream of the backwater zone"*	Characteristic flow depth $h_c = (C_f Q_c^2 / g w^2 S)^{\wedge}1/3$ (sensu Parker et al., 2007). C_f = bed friction coefficient, Q_c = characteristic water discharge, w = channel width, g = gravitational acceleration, S = slope.
Blum et al., 2013	Review	Slopes depicted in their Fig. 4B but without reference, no in-text comments	Slopes depicted in their Fig. 4B but without reference, no in-text comments	*"typically bankfull channel depth"*	No comment. Depths depicted in their Fig. 4B but without reference.	No comment. Depths depicted in their Fig. 4B but without reference.
Ganti et al., 2014	Huanghe river	*"Channel bed slope in the lower Huanghe reaches, from Luokou to Lijin"*. Upstream of backwater zone.	Range based on slopes measured the last 70 years. Method not mentioned.	Bankfull flow depth	One location, i.e. Lijin, 120 km from the shoreline. Estimated backwater length is 21–54 km.	Based on historical data published in previous publications.
Hartley et al., 2016	13 modern rivers, single thread, low gradient	*"…..between the bankfull elevation at the apex and te shoreline of each delta and cross-checked with the literature to ensure consistency."*	Channel bankfull slope from Digital Elevation Models from Shutle Radar Topography Mission	*"h_f is flow depth (typically bankfull channel depth)"*	*"for most examples include an average depth of the apex-shoreline length. Where this was not available, reliable depth measurements for portions of the river close to the apex were used"*	Published information or *"reliable depth measurements for portions of the river close to the apex were used"*
Ganti et al., 2016	Scaled physical experiments* and 8 modern delta rivers from Chatanantavet et al., 2012**	*"within the normal-flow zone"* * / *no comments***	**no comments	Normal-flow depth* / characteristic flow depth**	*"within the normal-flow zone"* * / no comments**	*"Measured flow depth computed by differencing the water surface profile and the bed surface profile within the confined portion of the experimental facility"* * / formula based on discharge (Parker)**
Fernandes et al., 2016	Mississippi and Rhine	Estimated in the normal flow reach (Mississippi river), more than one channel depth above mean sea level and upstream of backwater zone (Rhine river)	Water surface gradient in the normal flow reach (Mississippi river), channel belt gradients based on highest elevation of bar sand, taking into account sinuosity (Rhine river).	Mean channel depth	Rhine river: no comments, Mississippi river: upstream of CBK 300.	Low, intermediate and high values of mean normal flow depth were acquired from depths of filled oxboy lakes (Mississippi river) or channel belt thickness (Rhine river)
Gugliotta et al., 2017	Mekong river	Not applicable - (Lb is taken where sea level intersects the riverbed profile)	Not applicable - (Lb is taken where sea level intersects the riverbed profile).	Riverbed - no further comments (irrelevant as Lb is taken where sea level intersects the riverbed profile)	Lower 750 river kilometers, estimated backwater length is 560 km.	Riverbed elevations measured at 1-km intervals from hydrological atlases (Mekong River Commission and Ministry of Transport of Vietnam & Cambodia, in Oketani and Haruyama 2011)
Brooke et al., 2020	Steep rivers, Madagascar	Evaluated in the 25 km bin immediately	Measured from elevation change every 5 km and binned into 25 km segments,	Bankfull flow depth	Evaluated upstream of the avulsion site	*"…using the empirical bankfull Shields stress relation* (Trampush et al.,

(*continued on next page*)

Table 3 (*continued*)

Reference	Study type	Slope measurement location	Slope measurement method	Channel depth type	Channel depth measurement location	Depth measurement method
		upstream of the avulsion sites	based on digital elevation model from Shutle Radar Topography Mission 2000.			2014*) and the threshold channel theory for alluvial rivers (*Dunne and Jerolmack, 2018*). These independent methods yielded consistent bankfull flow depth values."*
Smith et al., 2020	Lower Trinity River, Texas	Based on an average across the lower 110 river kilometers (from Phillips et al., 2005)	From channel thalweg elevations (Phillips et al., 2005)	Average channel depth	Based on an average across the lower 110 river kilometers, estimated backwater length is 60 km.	From channel cross-sections from channel surveys (in Phillips et al., 2005)
Prasojo et al., 2021	105 modern deltas	No comments about location	Digital Elevation Models from Shutle Radar Topography Mission: Slope is calculated from the water elevation profile along the centerline of the main distributary channel.	Characteristic flow depth	"Qc (characteristic water discharge) is taken as close to the upstream limit of the delta as data availability allows"	Characteristic flow depth $h_c = (C_f Q_c^2 / g W_{av}^2 S)$^1/3 (sensu Parker et al., 2007). C_f = bed friction coefficient, Q_c = characteristic water discharge, W_{av} = channel width, g = gravitational acceleration, S = slope.
Brooke et al., 2022	Avulsion sites on modern rivers	No comments	From previous publications if available. If not, from the 15arc-sec resoltion HydroSHEDS DEM (Yamazaki et al., 2011) or based on channel-floodplain slope from a STRM and AW3D30 composite.	Bankfull flow depth	Upstream of the avulsion site	From previous publications if available. If not, then $h_{bf} = Max\ [0.5Q^{0.3}, 1.0]$. Q = long-term average water discharge (Trampush et al., 2014; Cohen et al., 2014). Validity of this equation was tested by comparing with bankfull flow depth estimates based empirically on bankfull Shields stress criterion.

Channel depth for backwater length estimates has previously been obtained along different segments of the river profile as well: i) 'upstream of the backwater zone', ii) 'evaluated upstream of the avulsion site', iii) 'as close to the upstream limit of the delta as data availability allows' iv) at one location only, v) across long stretches of the river path or vi) lack further specification (Table 3). Studies in which channel slope and depth are derived from datasets that cover the river path continuously over stretches longer than the backwater length are few (Nittrouer et al., 2011; Gugliotta et al., 2017). This reflects the efforts (e.g. bathymetric survey of hundreds of river km) needed to establish such continuous riverbed profiles. Obtaining channel depth from different segments of the river may lead to a ¬15% difference in backwater length calculation, based on results from the Mississippi River as an example (Fig. 4B, Table S4B).

Recommendations: Riverbed profiles typically show significant local variation and water surface slopes steepen in landward direction, inherent to the typical graded river profile (Mackin, 1948). Subsequently, slope and depth estimates from only one single location can't provide representative parameters. Therefore, the preferred method to estimate backwater length in modern rivers is to use datasets with channel slope and thalweg depth covering the river path over long enough distances to identify the point where the riverbed elevation intersects sea level (Nittrouer et al., 2011; Gugliotta et al., 2017). By doing so, the locally irregular riverbed profile is averaged over a longer section, and subjectivity and ambiguity in obtaining slope and depth from one or a few selected locations or a certain section of the river path are minimized. However, datasets with long profile river depths are scarce and will limit the application of such 'intersection method'. Therefore, estimating Lb indirectly by projecting channel thalweg along slope to the crossing point of the two lines (i.e. Lb = h/S) provides a commonly used alternative, but less accurate method. See section 5 for further discussion.

3.2. Backwater length estimates

Backwater length is measured along the river centerline in *river km* (Nittrouer et al., 2011; Blum et al., 2013; Smith et al., 2020) or as a straight distance to the coastline (Jerolmack, 2009, and in ancient settings), after defining where the riverbed intersects sea level or deriving it from h/S. However, most publications do not elaborate on how they measure this distance. The backwater length may be longer than the direct distance to the coastline where backwater length is measured in river kilometers and the river is sinuous. For example, the point on the map calculated as the upstream limit of the backwater length will be twice as far away from the coastline for a river with a sinuosity index of 2.0 when using a straight line compared to measuring in river km.

Recommendations: Authors should specify the distance annotation they use (i.e. river km or straight line from intersection to river mouth) and the use of different methods should be considered when comparing backwater estimates from different publications. Plotting straight line distances (i.e. a trigonometric approach) for previously estimated backwater lengths results in an upstream limit of backwater zones that are several hundred river km upstream of the actual riverbed intersection with sea level (Fig. 4C). Based on this, in addition to the omission of large-scale changes in river course if using a straight-line distance, we recommend using river km for consistence and correcting of sinuosity where applicable and known.

3.3. Channel depth type

Various channel depth types have been considered when estimating backwater lengths in modern river systems: i) characteristic flow depth,

Section 3.1. Location to measure slope and channel depth, Section 4.2. Backwater length estimates

A — Slope

Input location	Selected reference*	Input parameters based on bankfull discharge	depth (m)	Output: Slope	Output: Backwater length (km)
1. Between apex and shoreline	This study, following Hartley et al. 2016	19 m elevation at 490 river km 0 m elevation at 0 river km	31	3.88E-05	799
2. Normal flow reach	This study, following Fernandes et al. 2016	53 m elevation at 1050 river km 26 m elevation at 650 river km	31	6.75E-05	459
3. Upstream of avulsion site, across 25 km	This study, following Brooke et al. 2020	20 m elevation at 515 river km 19 m elevation at 490 river km	31	4.00E-05	775
4. Distances long compared to backwater length ♦	This study, following Paola and Mohrig 1999 ♦	54 m elevation at 1050 river km 0 m elevation at 0 river km	31	5.14E-05	603

B — Depth

Input location	Selected reference*	Input: Slope	Output: Channel depth (m)	Output: Backwater length (km)
Upstream of backwater zone	This study, following Chatanantavet et al. 2012	6.75E-05	26	385
Upstream of avulsion site	This study, following Brooke et al. 2020	6.75E-05	27	400
As close to the upstream limit of the delta as data availability allows	This study, following Prasojo et al. 2021	6.75E-05	29	430
Apex	This study, following Ganti et al. 2004	6.75E-05	29	430
Average depth over distances long compared to backwater length	This study, following Paola and Mohrig 1999	6.75E-05	31	459
Continuously, lower 1050 river kilometers	Nittrouer et al. 2011	6.75E-05	along river path	680**

C

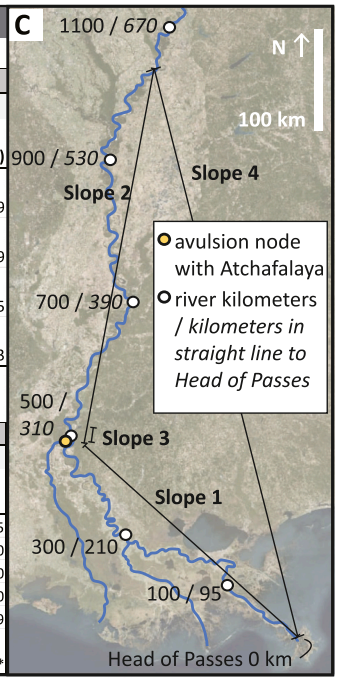

Section 3.3. Channel depth type

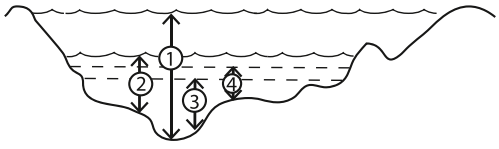

Type of channel depth	Selective reference*	Input: Slope	Output: Channel depth (m)	Output: Backwater length
1. Bankfull thalweg	Nittrouer et al. 2011	6.75E-05	31	459
2. Average depth (equals mean flow depth)	This study, following Bjerklie et al. 2018	6.75E-05	21	310
3. Average bankfull	This study, following Bridge & Tye, 2000	6.75E-05	16	237
4. Average bankfull	This study, following Long, 2021	6.75E-05	18	270

Section 3.5. Methods to obtain slope

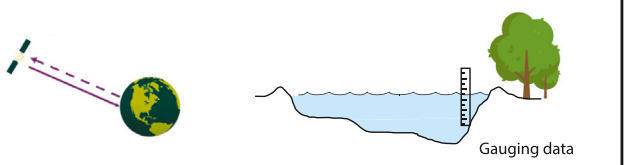

Input data	Selective reference*	Input: Channel depth (m)	Output: Slope	Output: Backwater length (km)
Gauging data: water elevation profile	Fig 2 in Nittrouer et al. 2011	31	6.75E-05	459
Digital elevation model	Following Hartley et al. 2016	31	7.25E-05	428

Section 3.4. Methods to obtain bankfull thalweg channel depth

Type of channel depth	Selective reference*	Input parameters	Input: Slope	Output: Channel depth (m)	Output: Backwater length (km)
Direct; riverbed survey	Nittrouer et al. 2011	River bed profile	6.75E-05	variable along river path	680**
Shields stress	This study - Mississippi river (used in Brooke et al. 2020 for rivers in Madagascar)	$\tau_{bf50}=(d_m S)/(PD_{50})$. D_m = mean bankfull channel depth, S = slope = 6.75*10-5, P = submerged dimensionless density = 1.65 g/cm3, D_{50} = average grainsize for lowermost portion of the channel = 280 µm, τ_{bf50}= Shields number for dimensionless shear stress = 1.86. The resultig mean bankfull chanel depth (15 m) needs to be converted to obtain bankfull thalweg channel depth with formula 7.	6.75E-05	17	256
River discharge	Prasojo et al. 2021	characteristic flow depth $h_c = (C_f Q_c^2 / g W_{av}^2 S)$^1/3 (*sensu* Parker, 2007). C_f = bed friction coefficient = 0.002, Q_c = characteristic water discharge = 33385 m3/s, W_{av} = channel width = 669 m, g = gravitational acceleration = 9.8 m/s2, S = slope = 6.75*10-5.	6.75E-05	20	290
Channel deposits	Fernandes et al. 2016	Filled oxbow lake deposits	6.75E-05	21	311
Literature	Hartley et al. 2016	Published information or *"reliable depth measurements for portions of the river close to the apex were used"*	6.75E-05	25	370

Fig. 4. Methods for input parameter acquisition (channel depth and slope) affecting the backwater length (Lb), focusing on error sources and definitions' ambiguity, using the Mississippi River as a case study for Lb = h/S estimation. The approach uses a representative value for one parameter (depth or slope) while keeping the other constant for comparison in backwater length estimates. A slope of $6.75*10^{-5}$, akin to the Mississippi River's water surface slope at bankfull stage, is applied (Nittrouer et al., 2011). When multiple publications have applied the same method, then a selected reference is listed. (A) Impact of using river segments to obtain slope, with constant depth. Note how slope obtained between the apex and shoreline gives the longest Lb. Locations are marked in C. ◆ It is unclear if Paola and Mohrig (1996) include the lower river reaches. (B) Impact of using river segments to obtain depth, with constant slope. **Note how all estimates result in shorter Lb than with the intersection method by Nittrouer et al. (2011). (C) Southern Louisiana, Mississippi River. The apex and avulsion node with the Atchafalaya River is marked. White marks indicate 200 river-km spacing. Straight-line distances (in Italics) to Head of Passes are significantly shorter than distances measured in river km. (D) Effect of varying channel depth methods on Mississippi River, yielding diverse depths and Lb estimates. Lb based on Lb = h/S with a slope of $6.75*10^{-5}$ for each Lb estimate. (E) Methods to infer bankfull thalweg depth result in backwater length differences ranging from 256 km to 680 km. (F) Slope estimates from digital elevation models or gauging data at bankfull stages demonstrates varied impact on Lb for the Mississippi River in normal flow reach. 31 m depth is applied for each Lb estimate (Fig. 2 in Nittrouer et al., 2011), to illustrate how variable slope estimates impact the resulting Lb. See Table 1 and Supplemental text S1 for additional explanation for A-F.

ii) normal flow depth, iii) bankfull flow depth, iv) average channel depth, and iii) channel depth without further specifications (Fig. 1, Table 3). Fernandes et al. (2016) estimates backwater length for low, intermediate, and high values of mean normal flow depth. Few publications specify exactly what they mean with their selected channel depth type. In modern rivers, mean flow depth and bankfull thalweg channel depth typically differ by a factor of ¬1.5 (Bjerklie et al., 2018). Using the Mississippi River as an example, the bankfull thalweg channel depth (i.e. 31 m) and average bankfull channel depth (i.e. 15.5 m, following Bridge and Tye (2000) who consider average bankfull depth as one-half of the bankfull thalweg channel depth) results in a backwater length of 459 km or 237 km, respectively (Fig. 4D, Table S3C).

Recommendations: Use of different channel depth types, is a source of error when estimating backwater length in modern river systems. When deciding which channel depth type to use, it is essential to consider the formative conditions for channel morphology, and clarify the terminology to eliminate ambiguity when discussing methods to obtain this parameter. We recommend using bankfull thalweg channel depth as the unit to calculate backwater estimates, because i) it represents formative flow conditions, ii) is the more standard and consistently measureable value, iii) is essential for assessing changes in sediment distribution and channel morphology as a consequence of changes in flow velocity in the backwater zone, iv) is the most transferable between modern and ancient systems, and v) avoids confusion (see section 2.2 for elaborated reasoning). Note that local deep scour holes should be excluded as these may exceed thalweg depth by a factor of two to three (Carey and Keller, 1957).

3.4. Methods to obtain bankfull thalweg channel depth

Channel depth for backwater length estimates in modern river systems can be measured directly from riverbed surveys and from channel deposits (Table 3). Channel depth inference as an unknown parameter has been achieved through empirical relationships using Shields stress based on grain size (Brooke et al., 2020) or river discharge (Chatanantavet et al., 2012; Prasojo et al., 2021), and channel width (e.g. Fielding and Crane, 1987; Gibling, 2006; Blum et al., 2013). Lastly, a few publications do not specify their methods to obtain channel depth (Table 3). Application of these methods by using the Mississippi River as an example and keeping slope constant, results in backwater lengths between 256 and 680 km, which equals a factor 2.6 difference (Fig. 4E, Table S3D).

Several publications list channel depth for the same rivers (Table 1, Table S1). These data (e.g., Hartley et al., 2016; Prasojo et al., 2021) facilitate comparison of channel depth estaimed for seven rivers inferred from empirical relationships with river discharge (following Parker et al., 2007; Prasojo et al., 2021) or based on an average depth over the apex-shoreline length but without a specified method (Hartley et al., 2016). Resulting channel depths are shallower based on the empirical discharge relationships for six out of seven rivers (Table S1). Chatanantavet et al. (2012) used the same discharge-based empirical relationships to estimate channel depth and analyzed five rivers also present in the dataset of Prasojo et al. (2021), of which three rivers have a shallower channel depth (up to 33%) than listed in Prasojo et al. (2021), despite using the same method (Table S1). A limitation of discharge-based empirical relationships is its dependence on the location of gauging stations, and the conversion needed to calculate characteristic water discharge from monthly discharge records. Channel belt depth (Fernandes et al., 2016) provides a similar depth as estimated by others (Chatanantavet et al., 2012; Prasojo et al., 2021) for the Mississippi River and a deeper channel depth for the Rhine-Muese River (Table S1).

Recommendations: When using river bed bathymetry or Shields' empirical relationship providing average channel depth (eq. 4), it is important to account for seasonal river level fluctuations and recalculate to bankfull conditions, if needed. For this, we recommend using:

$$D_{bf} = 1.502 \times d_{mf}^{0.9603} \quad (7)$$

with d_{bf} as bankfull thalweg channel depth, d_{mf} is mean flow depth, and $n = 6151$ (Long, 2021). Alternatively, bankfull thalweg channel depth can be estimated from channel width by using:

$$w_{bf} = 16.872\, d_{bf}^{1.169} \quad (8)$$

with d_{bf} is bankfull thalweg channel depth and W_{bf} is bankfull channel width. Channel width can be measured on aerial/satellite imagery.

Finally, bankfull thalweg channel depth can be inferred based on the empirical relationship with discharge and bed friction coefficient (Parker et al., 2007; Chatanantavet et al., 2012; Prasojo et al., 2021):

$$dbf = \left(\frac{CfQc2}{gWav2S}\right)^{1/3} \quad (9)$$

with d_{bf} is bankfull thalweg channel depth, C_f is bed friction coefficient, Q_c is the characteristic water discharge, g is the gravitational acceleration, W_{av} is channel width and S is slope.

Riverbed surveys resulting in absolute heights of the riverbed provide the most accurate sources of channel depth data, as no conversion is needed to obtain bankfull thalweg depths and it averages the locally irregular riverbed profile over a longer section.

3.5. Methods to obtain slope

Methods to obtain slope for backwater length estimates in modern river systems are predominantly twofold: i) using river water level elevation from digital elevation models (DEMs) or ii) direct measurements of water level elevation with respect to the riverbed (Table 3). Channel bed slope (Ganti et al., 2014) is rarely used, and several publications do not specify their data source (Table 3). When using direct measurements of river water level to obtain slope, temporal changes may influence water elevations and hence slope estimates. Discharge variations and tidal fluctuations cause differences in water levels, albeit that this occurs predominantly in the area of non-uniform flow, which is the backwater zone itself. Nittrouer et al. (2011) take such differences into account by averaging elevation data over 8 years.

Several publications list slope estimates for the same rivers (Table 1, Table S2) and differ up to a factor of 2. Such different results for the same river may result from measuring slope along different sections of the river path if using the same method (see section 3.1). We estimated slope over the same river segment based on gauge data and DEM for the normal flow reach of the Mississippi River, giving 7.25×10^{-5} and 6.75×10^{-5}, resulting in similar backwater length estimates of 428 km and 459 km, respectively (Fig. 4F, Table S3E).

Recommendations: River stage (i.e. low, normal, or high water level) and coastal dynamics such as daily to annual tides and wave conditions may affect the steepness of the water elevation profile which in turn impacts slope estimates. However, this will be mostly prominent in the area of non-uniform flow, i.e. the backwater zone, which implies that such differences only play a role when only collecting data from the backwater zone itself, should be avoided (Paola and Mohrig, 1996; Nittrouer et al., 2011; Fernandes et al., 2016). An advantage of DEMs is their global availability, contrasting the localized and scarcely available data sets with direct measurements of water surface elevation. However, they provide static snapshots and it is important to evaluate the contemporaneous river stage and its relation to bankfull, as the river path might be captured during multiple satellite orbits.

We consider both slope estimates derived from DEMs and direct measurements of water level or riverbed elevation equally recommendable for obtaining backwater length estimates in modern rivers. Note that the abovementioned slope methods provide channel slope and not valley slope (i.e. straight-line distance). Backwater length expressed as valley length must be corrected for river sinuosity where sinuosity is

high (see sections 4.1 and 4.2).

4. Workflows, error sources, and uncertainty ranges

4.1. Ancient settings – workflows to obtain backwater length

Four different workflows are proposed to estimate backwater lengths in ancient strata (workflow A1– A4, Fig. 5), based on different input data for obtaining bankfull thalweg channel depth and slope. They are arranged 1-to-4 in order of preference related to increasing error range (Fig. 6). Detailed recommendations on the collection and selection of input data can be found in section 2.

Workflow A1 and A2 both use grain size data to estimate slope but differ in their method to obtain bankfull thalweg channel depth (Fig. 5). Workflow A1 estimates bankfull thalweg channel depth (from story thickness (step A, Fig. 5) after decompaction (step B, Fig. 5) (Long, 2021). Workflow A2 determines bankfull thalweg channel depth based on average cross-set thickness (steps B, C, D, and E, Fig. 5). Cross-set thicknesses also require decompaction (step B). Mean dune height is then estimated (eq. 2; step C) and used to calculate *average* bankfull channel depth (eq. 3; step D). Finally, a conversion to *bankfull thalweg* channel depth is needed, for which we recommend using information about the channel cross-sectional shape to select the most accurate multiplier (see section 2.3, step E, Fig. 3). Slope is estimated using a representative sample of average bedload grain size (D50) and the average bankfull channel depth from both workflow A1 and A2 (eq. 4; steps F and G, Fig. 5).

Workflow A3 and A4 derive an estimate of slope based on bankfull channel width (w_{bf}) instead of grain size (cf. workflow A1 and A2, Fig. 5) and combine this with either bankfull thalweg channel depth from fully preserved channel story thickness (steps A and B, workflow A3, Fig. 5) or empirically based on average cross-set thickness (steps B, C, D and E, workflow A4, Fig. 5). Slope is estimated from bankfull channel width (w_{bf}) (eq. 6; steps G and H, Fig. 5). If no channel width data is available, bankfull width can be estimated from bankfull thalweg channel depth using $w_{bf} = 16.872\ d_{bf}^{1.169}$ (Long, 2021). If sinuosity (P) is known, we recommend using $w_{bf} = 16.293\ d_{bf}^{1.198}$ for low sinuosity rivers ($P < 1.3$), $w_{bf} = 17.338\ d_{bf}^{1.168}$ for intermediate ($1.3 < P > 1.7$), and $w_{bf} = 17.458\ d_{bf}^{1.230}$ for high sinuosity systems ($P > 1{,}7$) (Long, 2021).

Finally, note that resulting backwater lengths are in river kilometers.

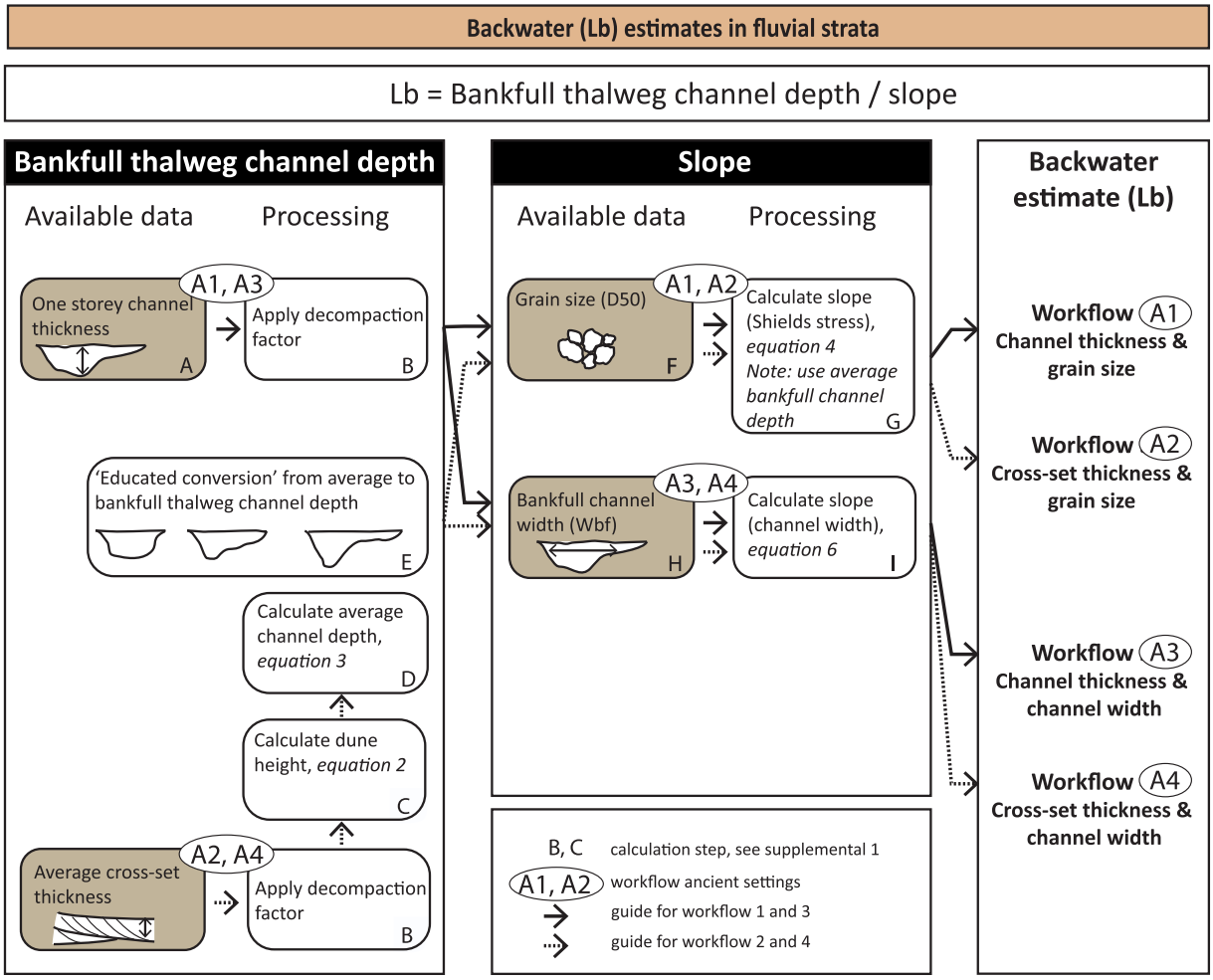

Fig. 5. Workflow recommendation for estimating backwater length (Lb) in ancient settings (A1–A4), based on different input data (brown boxes) to obtain bankfull thalweg channel depth and slope. Workflow numbers are annotated as well as data collection and/or calculation steps (A-H white boxes) that need to be executed (e.g. workflow A1 is based on steps A, B, F, and G) See Fig. 3 for elaboration on the educated conversion, step E. Note that the resulting backwater length is in river kilometers. A correction for sinuosity index is needed to estimate the straight-line distance from the paleoshoreline to the upstream limit of the backwater zone. See text for further discussion. Workflows are numbered in order of preference providing the data permits(see section 5.2). (For interpretation of the references to colour in this figure legend, the reader is referred to the web version of this article.)

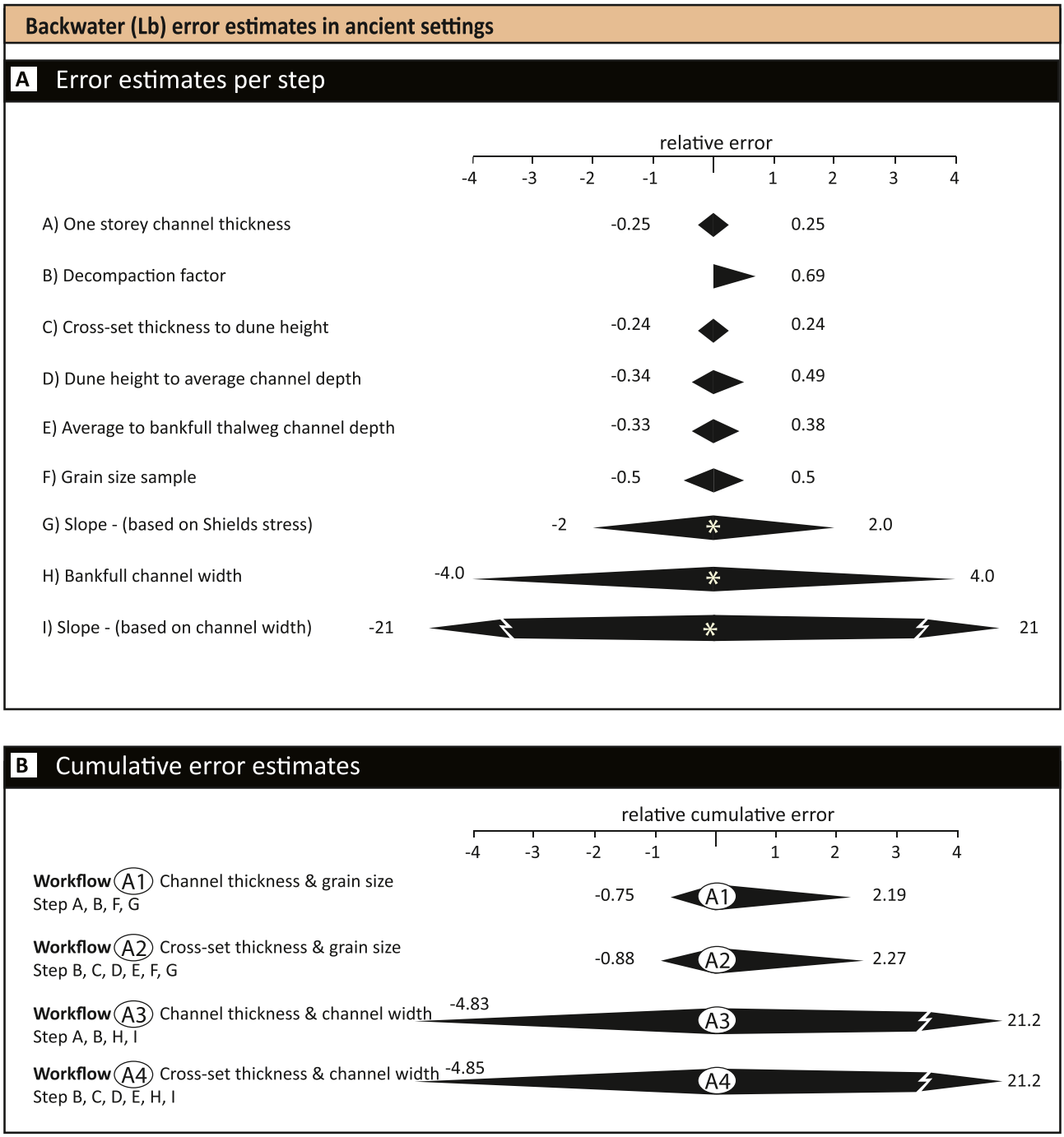

Fig. 6. Display of error magnitudes. (A) Estimated errors for each step or calculation used in the recommended workflows. Letters A-J relate to steps used in Fig. 5. The errors represent estimates that approximate the maximum generalized error of each step, and reflect a 50% (step D) or 95% (all other steps) confidence interval resulting from inherent scatter in previous established relationships or potential errors during data collection. * are depicted as error factors rather than relative errors. See Supplemental text S1 and S3 for more details. (B) Cumulative error estimates for each workflow are calculated by using an error propagation equation based on partial derivatives concerning the variable with the uncertainty. See Supplemental text S4 for calculation details and text (sections 2 and 4) for further discussion and references.

This is inherent to the method because the Shield's-based methods used to estimate slope from grain size yield channel slope rather than valley slope. However, in ancient settings backwater length estimates are commonly referred to as a straight-line distance from the paleoshoreline, neglecting distance differences arising from sinuosity. In cases where the studied system was sinuous, a correction for sinuosity is needed to estimate the true straight-line distance to the upstream limit of the backwater zone. We recommend using any of the common methods to estimate paleo sinuosity (Le Roux, 1992, 1994; Bridge et al., 2000; Ghosh, 2000) and correct the previous backwater length estimate (Lb) for sinuosity using $Lb_{\text{straight-line distance}} = Lb / \text{sinuosity index}$.

4.2. Ancient settings – error sources and uncertainty ranges

We utilize cumulative uncertainty estimates for prioritization of each workflow (see section 5.2). Each step within the workflows has an uncertainty range, due to natural scatter in previously established relationships and uncertainties in collection of (field) data parameters. Propagation of uncertainties affects cumulative uncertainty in backwater length estimates (Fig. 6).

Relative errors for individual steps (step A-H, Fig. 5) vary between 0.25 and 21 and result from uncertainties inherent to data collection and selection and empirical relationships' (Fig. 6, Supplemental text S2-S3) (Bridge and Mackey, 1993; Leclair and Bridge, 2001; Hajek and Wolinsky, 2012; Blum et al., 2013; Holbrook and Wanas, 2014; Bradley and Venditti, 2017; Bjerklie et al., 2018; Gingerich, 2019).

Combining all these uncertainties involved in the execution of a workflow provides cumulative errors, which may be evaluated by:

$$\frac{\Delta Q}{|Q|} = \sqrt{\left(\frac{\Delta a}{a}\right)^2 + \left(\frac{\Delta b}{b}\right)^2 + \ldots + \left(\frac{\Delta z}{z}\right)^2} \quad (10)$$

with $\Delta Q/|Q|$ being the cumulative relative error and $\Delta a/a$, $\Delta b/b$, etc. being the relative error of individual steps in the workflows (see Sup-

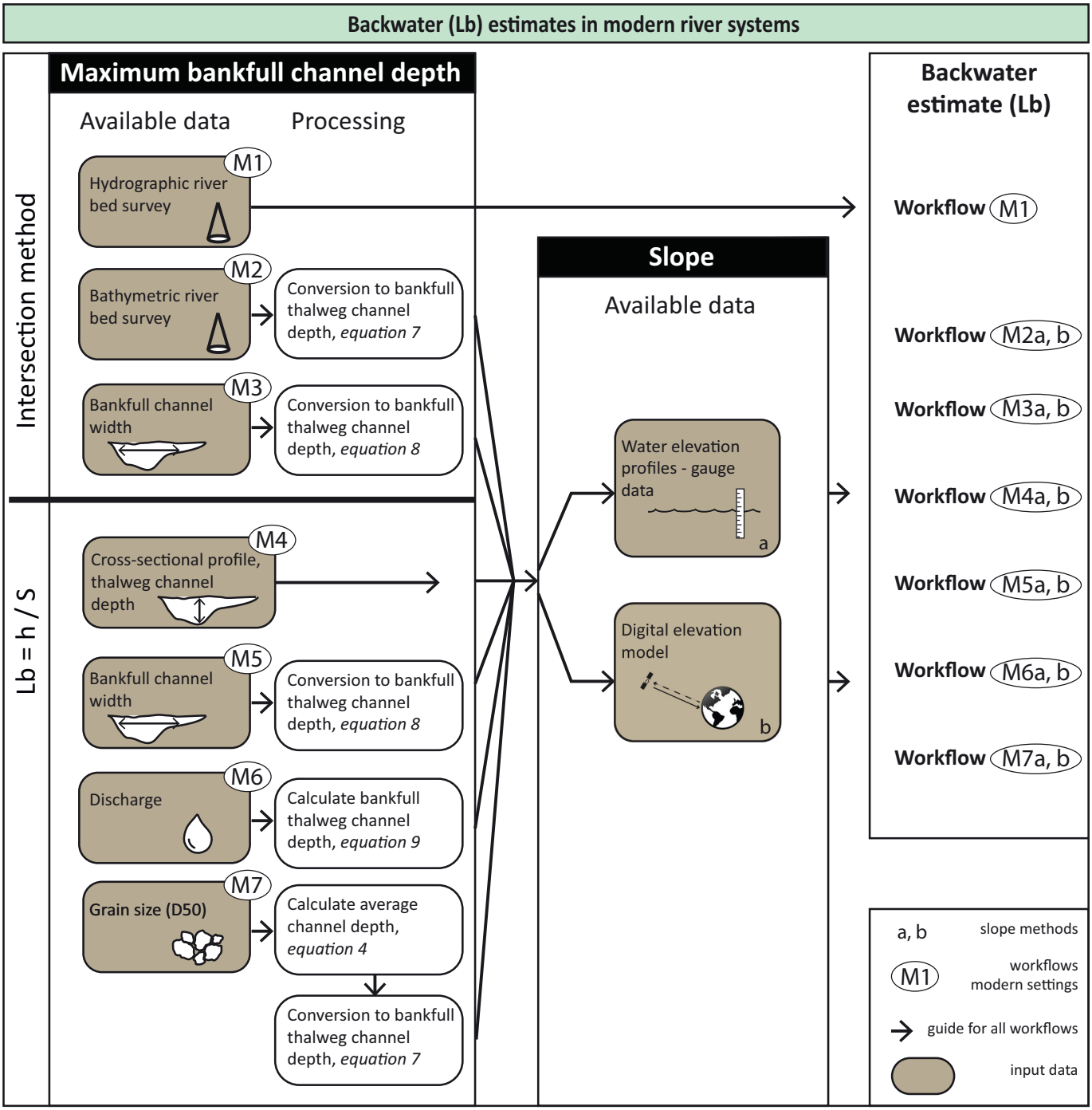

Fig. 7. Workflow recommendation for estimating backwater length (Lb) in modern river systems (M1–M7), based on different input data (brown boxes) to execute the intersection method or obtain bankfull thalweg channel from depth and slope. Workflow numbers reflect prioritization (see section 5.2). (For interpretation of the references to colour in this figure legend, the reader is referred to the web version of this article.)

plemental text S4). Cumulative relative errors range between 2.19 (workflow A1 and A2) and 21.2 (workflow A3 and A4) when comparing the proposed workflows for estimating backwater lengths in ancient settings (Fig. 6). For example, a backwater length estimate of 100 km obtained by applying workflow 1, has a minimum of 25 km (i.e. 100 km – (0.75 × 100)) and a maximum of 319 km (i.e. 100 km + (2.19 × 100)) when taking its uncertainty ranges into account. Backwater calculations appear most sensitive to errors in slope estimates.

4.3. Modern settings – workflows to obtain backwater length

Seven different workflows are proposed to estimate backwater lengths in modern river systems (M1–M7), based on quality of input data for bankfull thalweg depth and two methods to measure slope (Fig. 7). Detailed recommendations on the collection and selection of input data can be found in section 3.

There are two fundamental approaches to estimating the backwater length in modern systems, i) the the intersection method in which the distance between the river mouth and the location where riverbed elevation intersects sea level provides the backwater length (Nittrouer et al., 2011; Blum et al., 2013; Fernandes et al., 2016; Gugliotta et al., 2017; Smith et al., 2020) and ii) indirect estimates of backwater length (L_b) by calculating $L_b = h/S$, with h is bankfull thalweg channel depth and S is slope (Paola and Mohrig, 1996; Hartley et al., 2016; Ganti et al.,

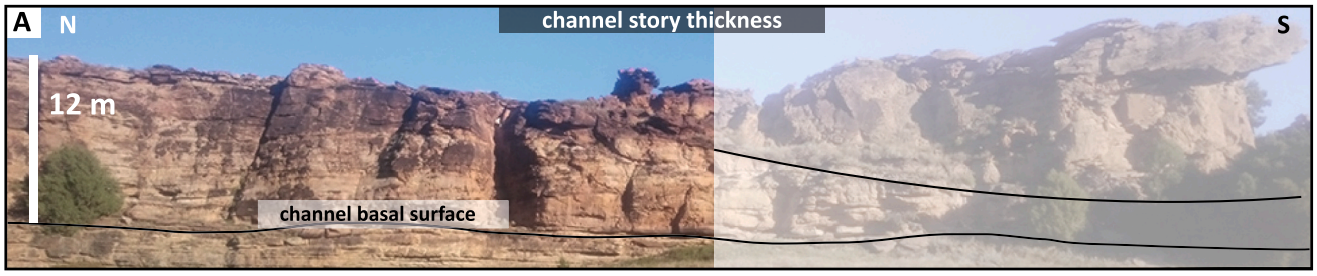

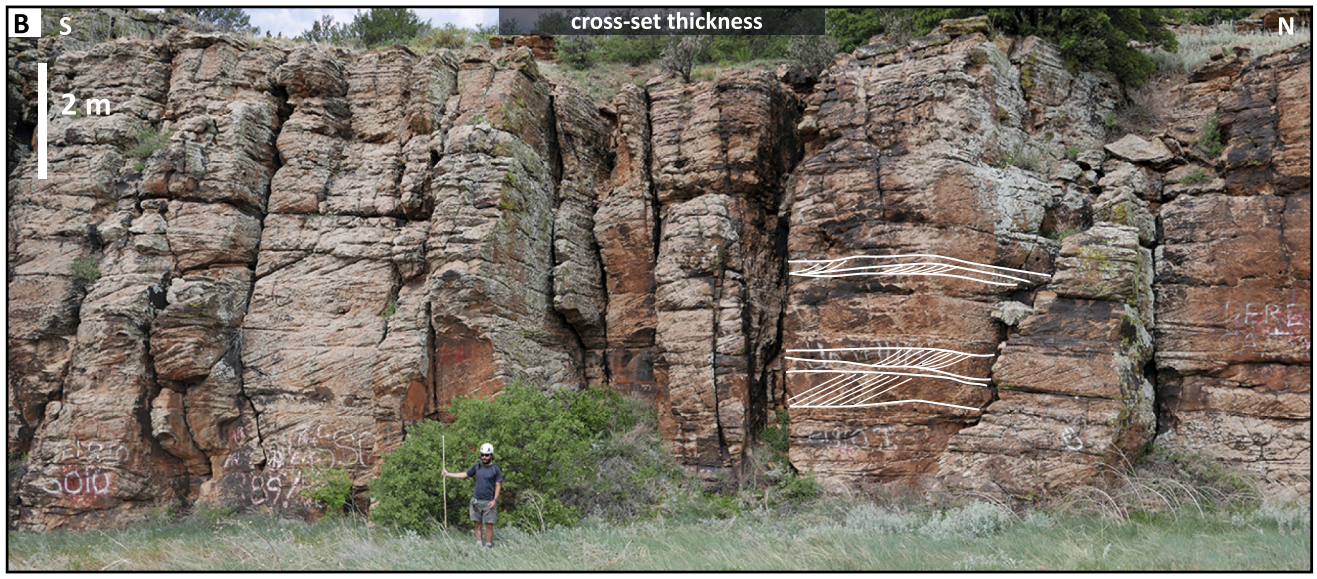

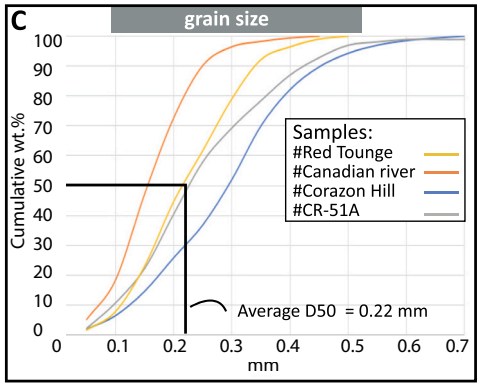

D

Input data			Output - Lb (km)		Output - Lb dimensionless	
			Lb (km)*	Lb (km)**	r/Lb♦	r/Lb♦♦
Workflow 1 (channel storey & grain size)		mean	188	188	1.0	1.0
bankfull thalweg depth from channel storey	13.2 m	max	599	326	3.2	1.7
slope from grainsize	7.02E-05	min	47	141	0.3	0.8
Workflow 2 (cross-set thickness & grain size)		mean	125	125	0.7	0.7
bankfull thalweg depth empirically from cross-sets	10.8 m	max	410	245	2.2	1.3
slope from grainsize	8.09E-05	min	14	59	0.1	0.3
Workflow 3 (channel storey & channel width)		mean	23	23	0.1	0.1
bankfull thalweg depth from channel storey	13.2 m	max	520	41	2.8	0.2
slope from channel width	5.64E-04	min	0	18	0.0	0.1
Workflow 4 (cross-set thickness & channel width)		mean	19	19	0.1	0.1
bankfull thalweg depth empirically from cross-sets	10.8 m	max	427	38	2.3	0.2
slope from channel width	5.64E-04	min	0	9	0.0	0.0

Fig. 8. Outcrop case study: examples of input parameters obtained from the lower Cretaceous Mesa Rica Sandstone (Van Yperen et al., 2021) used to estimate backwater length following all proposed workflows (A1–A4). (A) Single-story channel depths are on average 12 m thick in the depositional system. (B) Example of cross-stratified bed sets. (C) Particle size distribution curves for grain size samples from the lowermost bedforms from trunk channels. The average D50 based on these four samples is 0.22 mm. (D) Table listing input parameters used to apply all four workflows to estimate backwater length. See Table S4 for detailed calculations. Lb = backwater length, based on error propagation for obtaining both channel depth and slope* and only channel depth**. r/Lb = non-dimensionalized backwater length (Lb) concerning workflow A1, i.e. Lb from workflow A1 (Lb = 188 km) is given a value of 1, everything else is a departure from that. Cumulative errors are taken into account for both channel depth and slope◆, and only channel depth◆◆. The green box highlights non-dimensionalized distances depicted in Fig. 9. (For interpretation of the references to colour in this figure legend, the reader is referred to the web version of this article.)

2016; Brooke et al., 2020, 2021; Prasojo et al., 2021).

The intersection method implies that either the absolute height of the riverbed profile is measured directly with a hydrographic riverbed survey (workflow M1), or the channel depth is subtracted from the river water level elevation (workflows M2 and M3) (Figs. 6 and 7). The intersection method requires that bankfull thalweg channel depth and river slope are estimated over long distances. Workflow M1 uses the absolute height of the riverbed profile obtained with a hydrographic riverbed survey. The backwater length is where the riverbed profile intersects sea level and no slope profile is needed. In workflow M2, channel depth is measured directly with a bathymetric survey. As the conditions are unlikely to reflect bankfull conditions, the obtained channel depth needs to be converted to bankfull, for which eq. 7 is recommended. Workflow M3 allows for a desktop approach; channel width derived from satellite imagery over a long segment of the river profile can be used to obtain bankfull thalweg channel depth, using eq. 8. To find the riverbed/sea-level intersection, bankfull thalweg channel depth profiles obtained with workflows M2 and M3 should be combined with slope profiles from water elevation profiles (e.g. from gauge data) or digital elevation models (Figs. 7 and 8).

Backwater length estimates based on $L_b = h/S$ (i.e. workflows M4–M7*)* require bankfull thalweg channel depth (h) and slope (S) ideally measured in the normal flow reach, up dip of the backwater length, but still close enough to the beginning of the backwater length to be representative of flow conditions entering the backwater reach. This can be somewhat circular. For pragmatism, we suggest collecting input parameters at least some distance updip of the delta avulsion apex that is down dip of major tributaried or other flow disruptions (depth from at least one location, slope over long distances), as there is a presumed match between the location of the apex, backwater length and hence transition from normal flow to non-uniform flow conditions (Chatanantavet et al., 2012; Chadwick et al., 2019), albeit that rivers with backwater zones extending beyond the apex are common (Hartley et al., 2016). Workflow M4 obtains bankfull thalweg channel depth confidently updip of the backwater length from a cross-sectional profile (Fig. 7). Workflow M5 uses channel width from a similar location derived from satellite imagery which can empirically be converted into bankfull thalweg channel depth, using eq. 8 (Fig. 7). Workflow M6 estimates bankfull thalweg channel depth based on empirical relationships with discharge and bed friction coefficient using eq. 9 (Fig. 7). Finally, to obtain channel depth, workflow M7 uses channel bed grain-size data from the presumed normal flow reaches as an input parameter to utilize empirical relationships based on Shields stress, using eq. 4 (Fig. 7). Note that the resulting channel depth from this equation represents *average* channel depth and needs to be converted to bankfull thalweg channel depth using eq. 7 (Fig. 7, Table S3). Slope should be collected over long distances for workflows M4–M7, in the best-estimated normal flow reach from digital elevation models or based on water elevation profiles based on gauge data (A and B in Fig. 7). Combining bankfull thalweg channel depth and slope will provide backwater length estimates.

4.4. Modern settings – error sources and uncertainties

Assessment of cumulative uncertainty ranges for each workflow forms the base to prioritize workflow recommendations. However, most previously proposed workflows include one or several aspects or equations with unquantified uncertainty ranges or are based on data sets inaccessible for statistical analysis. As quantification of these is beyond the scope of this study, we only briefly list these uncertainties below.

Workflow M1 involves the performance of a hydrographic survey resulting in absolute elevation of the riverbed (Fig. 7). This workflow has minimal uncertainties, as the data is directly collected in the field and no data manipulation is needed to find the intersection with sea level. Error is only related to error in the measurement technique and estimation of the position of the thalweg trend. Workflow M2 is based on executing of a bathymetric survey to find channel depth along the river profile (Fig. 7). It assumes data collection at times of mean flow conditions and therefore involves conversion to bankfull thalweg channel depth. This conversion is empirical and is inherently prone to uncertainty ranges, albeit the r^2 value of this relation is remarkably high ($r^2 = 0.93$; Long, 2021). Workflows M3 and M5 utilize a channel width-to-depth ratio (Fig. 7). Such ratios should generally be considered approximate as they typically change in relation to channel style, sinuosity, system scale, tide-influence, climate, etc. (e.g. Leeder, 1973; Allen, 1986; Bridge and Mackey, 1993; Long, 2021). Workflow M4 obtains maximum bankfull depth from a cross-sectional profile, which will provide an accurate maximum bankfull depth for that particular location (Fig. 7). Workflow M6 uses the empirical relationship based on the characteristic water discharge, a bed friction coefficient, slope, and channel width to estimate maximum bankfull depth (Fig. 7) (Parker et al., 2007). Characteristic discharge is often calculated by taking the peak annual flood event with a two-year recurrence interval. The error imparted by this approach depends upon the recurrence period of the characteristic discharge, which varies widely from two years depending on the river conditions, particularly climate (e.g. Molnar et al., 2006; Hansford et al., 2020). In other cases, monthly discharge is converted to daily discharge using empirical transformations for different climates (Beck et al., 2018) which has an inherent scatter in its relationship. Additionally, selection of the bed friction coefficient and estimating slope and channel width will include uncertainties as well. Altogether, this suggests that the resulting channel depth is rather approximate. Workflow M7 uses average grain size (D_{50}) as an input parameter to an empirical relationship with Shields dimensionless shear stress, slope, average bankfull channel depth, and submerged dimensionless density. This involves uncertainty in collecting a sample representative for bedload transport and is inherent to estimating a characteristic slope from grain size, as well as error from channel depth (see Supplemental Text S2).

In general, we consider the intersection method (workflows M1–M3) more accurate than the indirect approach (i.e. Lb = h/S, workflows M4–M7) because of the abovementioned uncertainties in M4–M7, in addition to that the latter typically involves channel depth information derived from only one location, contrasting data collecting over long distances (i.e. the intersection method) which thereby smoothens the generally irregular riverbed profile and helps exclude error related to localized scour holes that roughen the bed profile.

5. Application of backwater length estimates

5.1. Testing the applicability and geological meaning of backwater estimate ranges with a modern and ancient example

5.1.1. Rock record case study – Dakota Group, USA

To test and illustrate the robustness of previously proposed workflows to obtain backwater estimates in ancient settings, we utilize the Cenomanian Mesa Rica Sandstone (Dakota Group, USA), which records fluvio-deltaic deposition in the Western Interior Basin and is exposed along a down-depositional dip 400 km transect in southeast Colorado and northeast New Mexico (e.g. Holbrook, 1996; Scott et al., 2004; Oboh-Ikuenobe et al., 2008; Van Yperen et al., 2019; van Yperen et al., 2021). Previous studies on channel deposits provide all the input parameters needed to estimate backwater length: grain size, bankfull thalweg channel depth and width, and average cross-set thickness collected in normal-flow reaches (van Yperen et al., 2021) (Fig. 8, Table S4). Architectural analysis indicates deposition by straight channels, based on the rare occurrence of point-bar deposits and predominant near-symmetrical channel cross-sections (Holbrook, 1996, 2001; Holbrook et al., 2006). Therefore, we use a multiplier of 1.1 to convert average to bankfull thalweg channel depth, and perform no correction for sinuosity to estimate the backwater length (see Table S4 for calculation details). Additionally, an outcrop-based assessment of the backwater length has previously been documented based on changes in

architectural style along the fully exposed fluvio-deltaic transect (Van Yperen et al., 2021). Along this transect, multivalley-sheet deposits transition downdip into a laterally continuous sheet of single-story trunk channel deposits (Holbrook, 1996, 2001) (Fig. 9). The latter result from significant avulsion and are therefore interpreted as evidence for deposition in the up-dip reaches of the backwater zone. This indicates a backwater length of ~180 km (Van Yperen et al., 2021). Other potential controlling factors on avulsion location, such as valley exit and/or bedslope-mediated avulsion (Hartley et al., 2016; Prasojo et al., 2021) are considered unlikely, as the Mesa Rica valley deposits are not incised into bedrock but in their alluvial plain for over 100 km further up dip of this transition and continuing to the shoreline. The multistorey channel infill results from temporal fluctuations in upstream sediment and water discharge (Holbrook, 2001).

The application of workflows A1–A4 (Fig. 5) based on these parameters shows that workflows A1 and A2 result in comparable backwater length estimates (i.e. mean Lb estimates of 188 km and 125 km, respectively), whereas workflows A3 and A4 have significantly lower mean Lb estimates (i.e. mean Lb estimates of 23 km and 19 km, respectively) (Fig. 8D, Table S5). The low values of workflows A3 and A4 are mainly owing to slope estimates inferred from bankfull channel width (workflows A3 and A4) being one factor higher than slope estimates based on grain size (workflows A1 and A2). Workflow A2 results in a shorter backwater length than workflow A1 because of a shallower bankfull thalweg channel depth and a slightly steeper slope. Additionally, we quantify an uncertainty range for each backwater length estimate by calculating the minimum and maximum Lb values in two ways: i) multiplication of propagated errors of both channel depth and slope (Lb* in Fig. 8, Table S5), and ii) multiplication of propagated errors in only channel depth estimates (Lb** in Fig. 8, Table S5).

Comparison of backwater length estimates and their uncertainty ranges with field-based observations suggests: i) changes in fluvial architectural style interpreted as linked to backwater conditions in the Mesa Rica Sandstone depositional system occur at up-dip length of ~180 km from the equivalent paleoshoreline (Van Yperen et al., 2021), which coincides closely with *mean* estimates of backwater length resulting from workflow A1 (188 km) and A2 (125 km), but far off (~9×) mean estimates following workflows A3 and A4. ii) *Maximum*

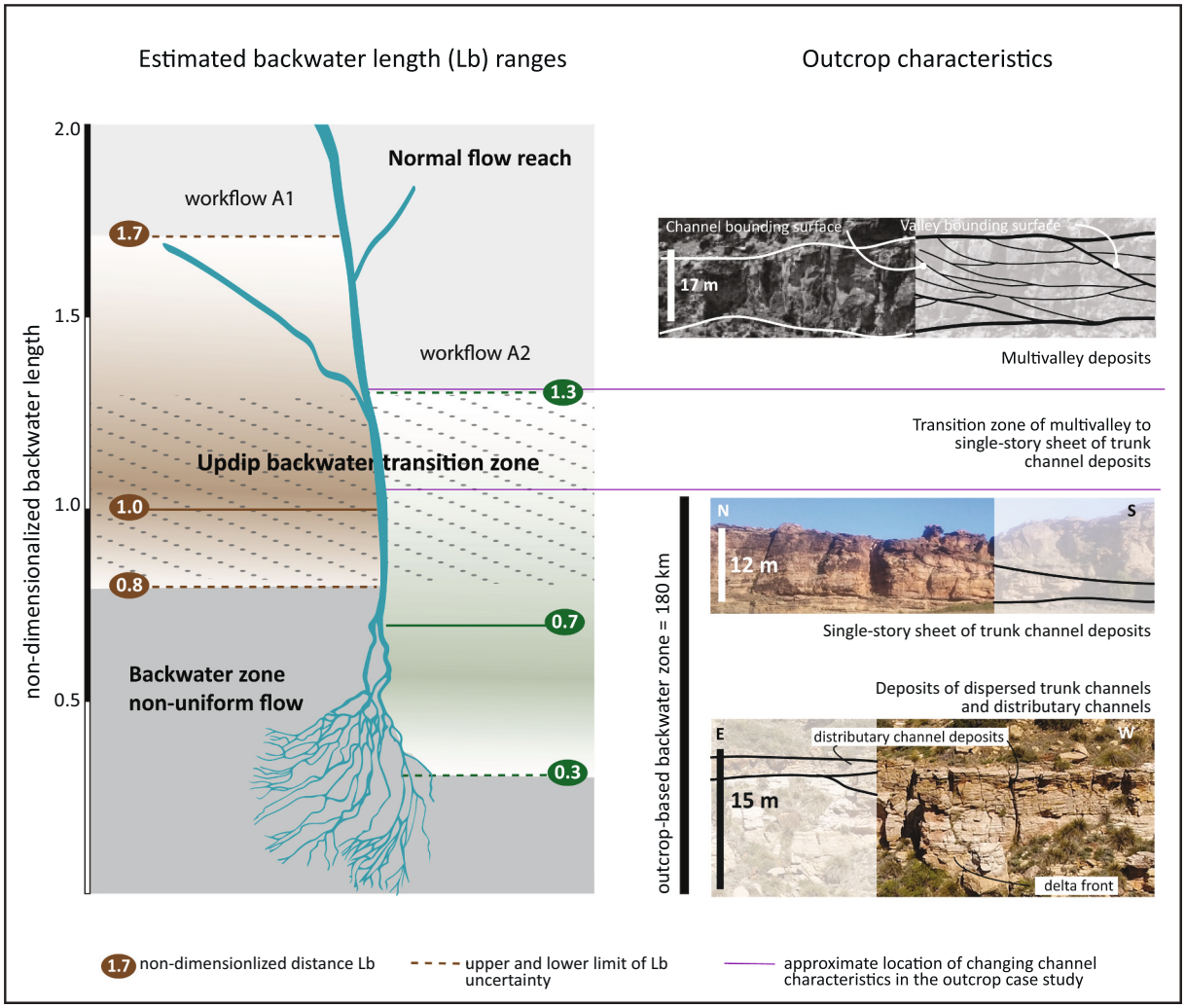

Fig. 9. Dimensionless backwater length estimates resulting from workflow A1 (in brown) and A2 (in green) projected onto a schematic representation of the ancient fluvio-deltaic depositional system selected as a case study (Cretaceous Mesa Rica Sandstone, USA). Lower, mean, and upper values of backwater length estimates are non-dimensionalized with respect to the mean backwater length from workflow A1. I.e. Lb from workflow A1 (Lb = 188 km) is given a value of 1, everything else is a departure from that. The overlapping (shaded) area represents the dimensionless up-dip backwater transition zone, where results from the two workflows overlap and represent the most reliable estimate of the up-dip limit of the backwater zone. Outcrop characteristics representing a summary of the main fluvial architectural styles ((Holbrook, 1996, 2001; Van Yperen et al., 2019) present in the case study are relevant to assess whether there is an actual link between backwater estimates and observable changes in fluvial architecture. Outcrop pictures modified from Holbrook (2001), van Yperen et al. (2021). (For interpretation of the references to colour in this figure legend, the reader is referred to the web version of this article.)

backwater lengths resulting from uncertainty ranges in both channel depth and slope for workflows A1 and A2 (i.e. Lb* is 599 km and 410 km, respectively) (Fig. 8D, Table S5) occur in an area along the depositional profile where multivalley channel deposits dominate the fluvial architectural style, and incision and aggradation patterns in stacked channel belts have no correspondence with down-dip base-level trends (Holbrook, 2001; Van Yperen, et al. 2021). No significant changes in channel architectural style are documented in this area. Consequently, the propagated error from both channel depth and slope estimates provides unrealistic values and we therefore recommend calculating uncertainty ranges based on only channel depth estimate uncertainties.

Finally, we use the minimum and maximum backwater length values to establish the 'up-dip backwater transition zone' based on the results of workflows A1 and A2 (see Fig. 9). In this zone, there is an overlap of the derived backwater length estimates and their uncertainty ranges. The lower and upper limit of this zone is defined by the lower limit of the backwater length estimate of workflow A1, and the upper limit of the backwater length of workflow A2, and contains the occurrence of changes in channel architectural style. We argue that the dimensionless up-dip backwater transition zone represents the most reliable estimate of the up-dip limit of the backwater zone and is potentially applicable to other systems as well. However, to further refine and test this dimensionless up-dip backwater transition zone, more outcrop studies in other systems are needed in which all workflows are calculated and compared

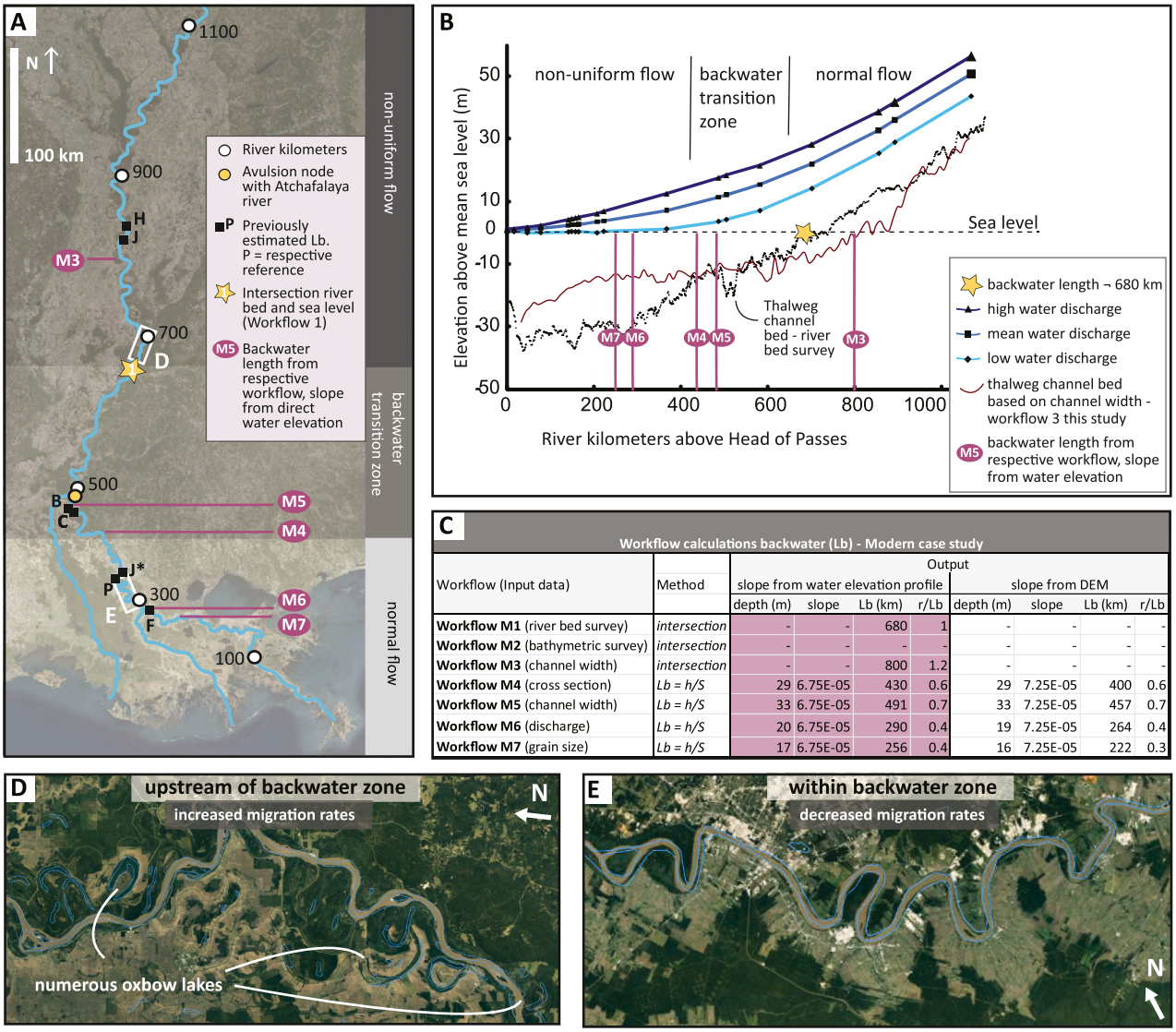

Workflow (Input data)	Method	Output: slope from water elevation profile depth (m)	slope	Lb (km)	r/Lb	slope from DEM depth (m)	slope	Lb (km)	r/Lb
Workflow M1 (river bed survey)	*intersection*	-	-	680	1	-	-	-	-
Workflow M2 (bathymetric survey)	*intersection*	-	-	-	-	-	-	-	-
Workflow M3 (channel width)	*intersection*	-	-	800	1.2	-	-	-	-
Workflow M4 (cross section)	*Lb = h/S*	29	6.75E-05	430	0.6	29	7.25E-05	400	0.6
Workflow M5 (channel width)	*Lb = h/S*	33	6.75E-05	491	0.7	33	7.25E-05	457	0.7
Workflow M6 (discharge)	*Lb = h/S*	20	6.75E-05	290	0.4	19	7.25E-05	264	0.4
Workflow M7 (grain size)	*Lb = h/S*	17	6.75E-05	256	0.4	16	7.25E-05	222	0.3

Fig. 10. Case study on the Mississippi River: (A) Lower 1100 river km of the Mississippi River with previously published estimations of the landward extent of backwater length, and all seven workflows proposed in this study (M1–M7). Previously published backwater lengths: J = Table 1 in Jerolmack (2009), J* = Fig. 14 in Jerolmack (2009), C = Chatanantavet et al. (2012); F = Fernandes et al. (2016); H = Hartley et al. (2016), P = Prasojo et al. (2021). (B) The intersection method (workflow M1) results in a backwater length of 680 km (modified after Nittrouer et al., 2012). Upstream of this, the thalweg channel bed slope and water surface slopes at different discharges are subequal to each other which is characteristic of normal flow reach. An up-dip backwater transition zone occurs between ~400 and ~ 700 river km (Nittrouer et al., 2012). Backwater lengths resulting from workflows M4–7 are projected onto the profile. (C) Input data, method, and resulting bankfull channel depth for each workflow. Note that workflows M4–7 are performed twice, with slope derived in the normal flow reach from the bankfull water elevation profile from gauge data (USACE, 1935; Nittrouer et al., 2011) and Digital Elevation Model (DEM). As results are similar, only backwater lengths based on slope estimates from water elevation profiles are depicted. See 3.5 and Table S4 for additional details. (D) and (E) exemplify the abundance and absence of oxbow lakes close to the upstream limit of the backwater zone (D) and within the backwater zone (E), respectively. A further narrowing of the channel belt just downdip of inset (E) has been assigned to avulsion-driven bifurcation rather than backwater effects (Gugliotta and Saito, 2019).

with changes in fluvial architectural style.

5.1.2. Modern case study - Mississippi River

We selected the Mississippi River (USA) to test and illustrate the proposed workflows for obtaining backwater length in modern river systems because of the availability of a continuous channel bed profile and water elevation profiles at different discharge stages in its lower 1050 river km (Nittrouer et al., 2011). Additional input parameters such as discharge (Prasojo et al., 2021), grain size and cross-sectional profiles (Nittrouer et al., 2012), and bankfull channel width are available or can be easily derived from satellite imagery.

All workflows, except M2, were testable using this data. Workflow M1 directly identifies the intersection between thalweg depth and sea level, occurring approximately 680 river km above Head of Passes and correlating with changes in flow conditions (Fig. 10A, B). The river bed profile based on width: depth ratios (workflow M3) intersects with sea level around 700 km (Fig. 10A, B, Table S5, S6). Workflows M4–M7 obtain backwater length estimates indirectly (i.e. Lb = h/S) and use slope collected in the normal reach area (i.e. 650–1050 km) based on water elevation profiles derived from both DEM and bankfull discharge stage. Backwater length estimates based on bankfull thalweg channel depth derived from a cross-sectional profile and width: depth ratio (Workflows M4 and M5, respectively) plot in the backwater transition zone. Conversely, estimates derived from discharge and grain size (Workflows M6 and M7, respectively) plot in the non-uniform flow zone (Fig. 10B, C). Previously published backwater length estimates based on h/S also plot in the non-uniform flow zone and backwater transition zone (i.e. between 281 and 480 km, see Table 1).

All backwater length estimates derived indirectly with Lb = h/S (workflows M4–M7, Lb between 222 and 491 river km) are significantly shorter than the 680 river km at which the riverbed intersects sea level and where the flow-type transitions from uniform to non-uniform (Fig. 10A-C, Table S5). This mismatch may result from different causes. Firstly, the input parameters may not be representative because the derived backwater length estimates are all shorter than the intersection length. This implies that either the input parameter for bankfull thalweg depth is too shallow, the slope is too steep, or both. The first seems unlikely, as we reason that the recommended use of bankfull *thalweg* channel depth already ensures maximum channel depths. Alternatively, lower slopes could be obtained by using a slope based on the full river profile (from updip to river mouth) instead of retrieved from the normal reach (as used in our case study on the Mississippi river), and will consequently result in longer backwater estimates.

We compared the various backwater length estimates to the location of previously documented changes in sedimentary trends and channel morphology. Particularly, backwater lengths were compared to a) a progressive decrease of channel-belt width/thickness ratio in the transition zone, between ~200–650 km (Blum et al., 2013; Fernandes et al., 2016) (Fig. 11A), b) coarsening grain size and channel bed aggradation in the transition zone (~500–600 river km) followed by distinct downstream fining (USACE, 1935; Nittrouer, 2013) (Fig. 11B), and c) increased migration rates between 400 and 800 river kilometers followed by a distinct decrease (Hudson and Kesel, 2000; Nittrouer et al., 2012; Fernandes et al., 2016) (Fig. 11A, B). The latter is illustrated by an increase in oxbow lake abundance, for example (Fig. 10 D, E). Contrastingly, channel belt and bar thickness analysis analysis (Fernandes et al., 2016; Martin et al., 2018) reveals only significant changes between 200 and 400 river km. In short, the intersection between riverbed and sea level (at ~680 river km) coincides approximately with the updip extent of the river segment that is characterized by each of the aforementioned changes except the increase of channel belt thickness. This contrasts indirectly derived backwater length estimates (Lb = h/S) resulting from workflows M4–M7 and previously published values which are shorter and plot outside or in the lower reaches of the zone of change (between 222 and 491 km) (Fig. 11C). Reaches updip of the backwater zone as estimated by intersection with the channel bottom are known to be impacted primarily by local tectonics and climate changes in the drainage instead of sea level (e.g., Holbrook et al., 2006; Rittenour et al., 2007; Blum et al., 2013).

A remaining question is to what extent backwater dynamics drive the previously mentioned changes in morpho-sedimentary channel characteristics of the Mississippi River or whether other factors play a role too. Hartley et al. (2016) identify a Pleistocene valley exit at around 500 river kilometers from Head of Passes, which matches the main avulsion node of the Mississippi River, onset in decreasing migration rates, increasing channel belt thickness, and grain size decrease (Fig. 11) (USACE, 1935; Hudson and Kesel, 2000; Nittrouer et al., 2012; Blum et al., 2013; Fernandes et al., 2016). This is not a bedrock valley exit, but Pleistocene fluvial terraces are emergent upstream and no longer onlapped by Holocene transgressive floodplain aggradation (Rittenour et al., 2007; Blum et al., 2013). This lapping relationship is considered backwater controlled (Blum et al., 2013), and the terraces are alluvial and not likely restricting lateral migration. ~200 km upstream of the Holocene onlapping onto the Pleistocene terraces changes in channel belt width, increased lateral migration rates, and grain size coarsening occur, which matches the current backwater transition zone (Fig. 11). Approximate coincidence between some morpho-sedimentary changes in the Holocene channel belt and the onlap point onto the Pleistocene terraces is thus likely a coincidence mostly of a common backwater cause. Erosion of the terraces is a good source of bedload material, however, so this secondary feedback to the Holocene Mississippi River where the Pleistocene channels emerge cannot be fully excluded as an influence.

Finally, testing of the causal relationship between estimated backwater length and actual changes in channel morphology and sedimentary trends is far from finished. We recommend extending the investigation of whether the riverbed/sea level intersection or derived Lb estimates match with morpho-sedimentary changes in other river systems.

5.2. Workflow recommendations

5.2.1. Ancient settings

We consider the mean backwater length of workflow A1 and maximum backwater length of workflow A2 as the most realistic estimates of the four proposed, as they are most closely related to observable outcrop changes in fluvial architectural style that are likely related to backwater effects (Fig. 9).

In ancient strata, four workflows are proposed (A1-A4) (Fig. 5) and tested (Fig. 8). Subsequently, workflows A3 and A4 are discarded based on i) the high uncertainty ranges resulting from using channel width as an input parameter to obtain slope and ii) the mean values providing backwater lengths that are considered too short to be realistic based on field-evidence from the case study (see *5.1.1*). Workflows A1 and A2 both use slope estimates derived from representative grain size samples to be used in empirical relationships based on Shields stress. In case grain size samples are not available, we recommend using the backwater length maximum value of workflow A4, as this is closest to the results of workflows A1 and A2 (Fig. 8D).

When input data for both workflows A1 and A2 is available, we recommend obtaining the input parameter bankfull thalweg channel depth from fully preserved channel story thickness (i.e. workflow A1), as this provides smaller uncertainty ranges than bankfull thalweg channel depth inferred from average cross-set thickness (i.e. workflow A2). In case of well data, we recommend the use of cross-set thickness (i.e. workflow A2), as assessment of proximity to channel axis and/or thalweg might be difficult. Finally, it is important to note that resulting backwater length estimates are in river kilometers. If the available data suggests a sinuous river system, the backwater length estimate should be corrected for sinuosity to acquire a straight-line distance from paleoshoreline to the linear upstream limit of the backwater zone (see 4.2).

The cumulative uncertainty for each backwater length estimate

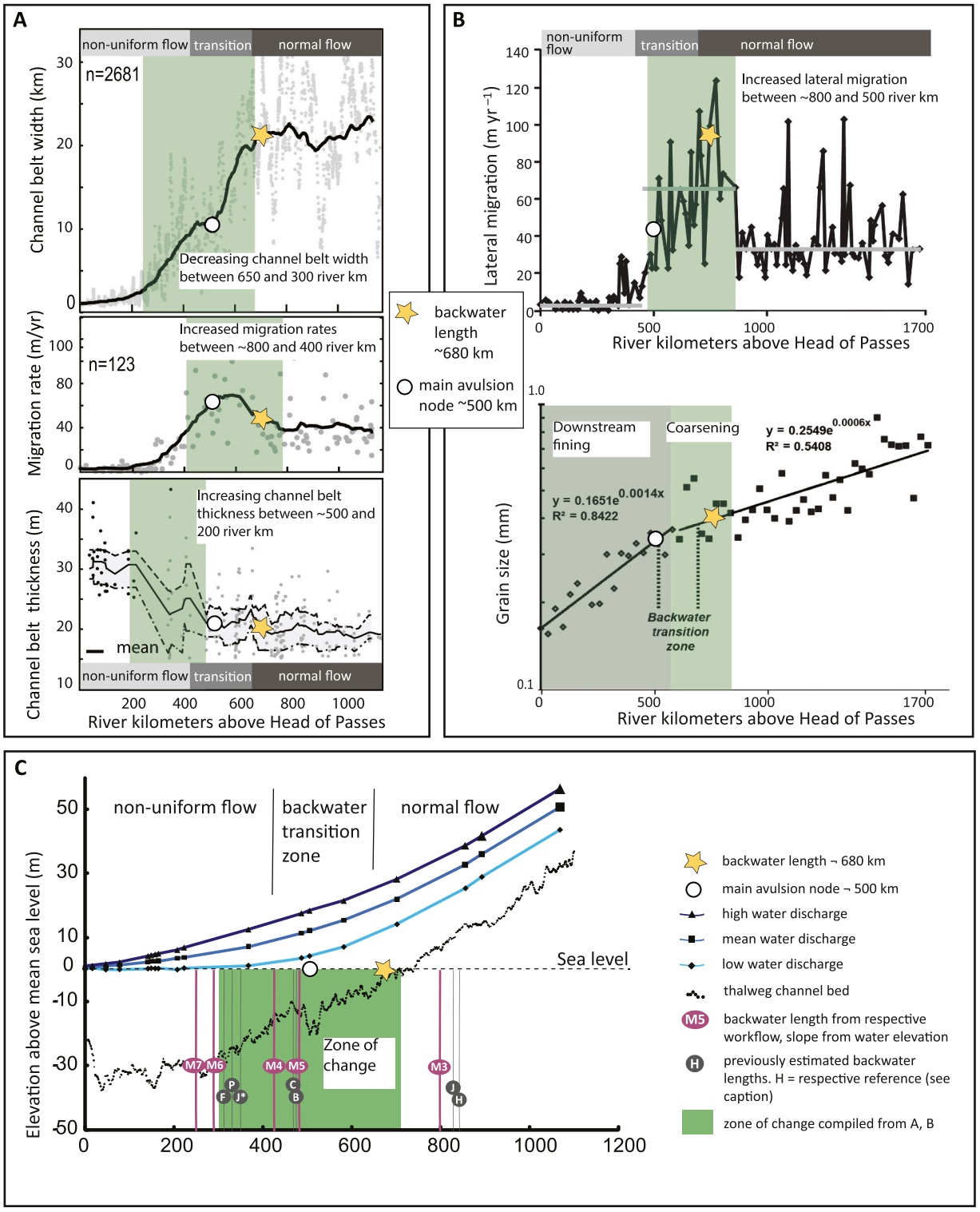

Fig. 11. Documented changes in sedimentary trends and channel morphology and their position along the lower Mississippi River. Green boxes highlight the zones characterized by changes. Location of the main avulsion node matches Holocene onlapping onto Pleistocene terraces. A) Channel-belt width, channel migration rates, and thickness of channel-belt deposits (Hudson and Kesel, 2000; Blum et al., 2013; Fernandes et al., 2016). Average values in black. B) Lateral migration for the lower Mississippi River (Hudson and Kesel, 2000; Nittrouer et al., 2012). Changes in rates of lateral mobility coincide with the regions changing grain size (modified after USACE, 1935; Nittrouer, 2013). C) Compilation of backwater length estimates resulting from different workflows and previously documented changes in sedimentary trends and channel morphology projected onto the bankfull water elevation profiles and thalweg channel bed profile (modified after Nittrouer et al., 2012). The zone characterized by these changes is depicted as a 'zone of change'. J = Table 1 in Jerolmack (2009), J* = Fig. 9 and 14 in Jerolmack (2009), B = Brooke et al. (2021), C = Chatanantavet et al. (2012); F = Fernandes et al. (2016); H = Hartley et al. (2016), P = Prasojo et al. (2020). See Table 1 for Lb estimates. (For interpretation of the references to colour in this figure legend, the reader is referred to the web version of this article.)

provides minimum and maximum values that can be used to establish the up-dip backwater transition zone (Fig. 9). In this zone, derived backwater length estimates and their uncertainty ranges overlap and thereby represent the most reliable range estimate of the up-dip limit of the backwater zone. To estimate these cumulative uncertainty ranges, we propose to neglect the slope uncertainties (see also 5.1.1). We believe this is a valid approach because i) slope is generally a difficult parameter to resolve in ancient successions (Long, 2021) and different methods may result in slopes that vary up to two orders of magnitude, ii) it is more likely that the relationship between grain size and slope represents steepness near the mean value than slopes far away from the mean value, iii) the case study presented here (Cretaceous Mesa Rica Sandstone, USA) shows that the maximum backwater length estimates based on error estimates that exclude slope uncertainties do not relate to any changes in fluvial style (Fig. 9) and occur in an area with basal channel scour depths up to teens of meters (or multiple channel-thicknesses) above the lowermost channel fills. This implies they aggraded well above sea level and are well up-dip of the backwater length. Considering an additional uncertainty factor for slope estimates of ± 2 in this case would give values that have no geological meaning beyond the error already imposed by channel thickness estimates. Further testing however is warranted to see if this trend is represented across comparable ancient systems.

Finally, input data must be representative for values averaged over length scales that are significant relative to the backwater length itself. Sampling across larger populations of channel stories provide inputs of more representative thickness and grain size values and guard against erroneous results derived from estimates based on sampling from extreme outliers.

5.2.2. Modern river systems

In modern fluvial systems, we propose and test seven workflows to obtain backwater length estimates (Fig. 7). Of these, workflows M1–M3 apply the intersection method, and Workflows M4–M7 provide backwater lengths based on Lb = h/S. The workflow recommendation is based on i) accuracy, ii) application of the proposed workflows (i.e. Mississippi case study), and iii) outcomes from assessing individual aspects and methods to obtain input parameters (section 3).

We recommend using the intersection method because it i) has the least uncertainties when using direct field data (i.e. workflow M1, hydrographic surface to obtain absolute height of the riverbed profile), ii) minimizes challenges and ambiguity in obtaining slope and depth from one or a few selected locations, iii) it averages the locally irregular riverbed profile over a longer section, and iv) better predicts changes in flow conditions, hydrodynamics, sedimentary trends and channel morphology related to backwater length (Wright and Parker, 2005; Nittrouer et al., 2011, 2012; Smith et al., 2020).

For application of workflows M4–M7, we recommend obtaining bankfull thalweg channel depth from the normal reach, estimated by measurements at least up-dip of the delta apex. Workflow M5 offers a convenient desktop approach, as bankfull thalweg channel depth is inferred from its empirical ratio with bankfull channel width, which can be easily derived from satellite imagery. However, even though workflow M5 results in a backwater length closest to the actual intersection point in the Mississippi case study (Fig. 10), we believe this might be by chance as width: depth ratios are highly variable and only approximate depth. Therefore, we consider that the use of a cross-sectional profile (workflow M4) provides the most accurate bankfull thalweg channel depth. It is important to bear in mind that the accuracy of Lb based on h/S depends on the representativeness of the obtained bankfull thalweg channel depth (i.e. h) and slope (i.e. S) parameters. Additionally, application to the Mississippi River showed that resulting backwater lengths are generally short when comparing the actual riverbed/sea-level intersection with backwater length estimates based on discharge and grain size (i.e. workflows M6 and M7), the latter plotting well into the non-uniform flow reach.

In summary, we recommend the following order of workflows, based on resulting backwater estimates closest to the actual intersection between riverbed and sea level based on the Mississippi River case study: Workflows M1, M2, and M4. Care should be taken when applying any of the other workflows, as workflows M3 and M5 use channel width: depth ratios, which tend to be highly approximate, and workflows M6 and M7 (based on discharge and grain size, respectively) tend to plot in the lower reaches of the backwater zone.

5.3. Backwater length estimates in modern versus ancient settings

Backwater length estimates in modern versus ancient setting bear some fundamental differences in best approach and geological meaning. Among the studied publications for this review, a match between changes in flow conditions, i.e. transition into the backwater zone, and intersection of the river bed with sea level has been demonstrated in the Mississippi and Trinity rivers (Nittrouer et al., 2011; Smith et al., 2020). Backwater lengths obtained in a modern river system can be measured directly by assessing this riverbed/sea-level intersection and the distance from that point to the river mouth. This contrasts the approach for ancient settings, in which Lb = h/S is based on parameters obtained in one or a few locations and depends on preserved proxies. The advantages of the intersection method are i) it has the least uncertainties regarding input data, ii) it discards ambiguity introduced by obtaining slope and depth from one or a few selective locations for slope or channel depth measurements, and iii) it averages the locally irregular riverbed profile over a longer section. In ancient systems, workflows targeting the full river profile are unrealistic. Moreover, pinpointing the up-dip extent of the backwater zone in ancient strata is ideally linked to evidence on the coeval paleoshoreline, hence dependent on accuracy of correlation and completeness of the stratigraphic record.

The backwater zone is dynamic over time. Its downstream termination and backwater-scaled avulsion-sites migrate in concert with shoreline evolution (Ganti et al., 2014; Brooke et al., 2021). Its upstream extent changes as up-dip influences change river discharge and thus channel depth. This causes another difference between backwater length estimates in modern versus ancient settings; the backwater length calculated for an ancient stratigraphic layer is not a discrete length for a discrete channel, as may be the case in the modern, but is instead a range of backwater lengths that incorporates changes in variabilities impacting backwater length between these multiple preserved channels. Each channel story in a stratigraphic layer represents only one spatiotemporal sample of some past river at that location recorded over some brief time (e.g., up to $\sim 10^1$ yrs), though collectively the sum of these stories over the extent of the layer will record much longer durations (e.g., millions of years) (see Holbrook and Miall, 2020). Therefore, a discrete backwater-length value is rarely applicable for an ancient stratigraphic unit, but rather is best represented by a range of mean and standard deviation from some broader sampling of a representative collection of channel stories in the layer.

Finally, preservational bias may impact backwater calculations in ancient settings as well. In high-accommodation systems, coastal progradation and retrogradation may be represented by downstream and upstream shifting of fluvial profiles preserved throughout a vertical succession (Shiers et al., 2018). In low-accommodation systems, however, limited space may cause advancement of the fluvial system over previously deposited strata, eroding some of the earliest deposits related to the backwater effect (Van Yperen et al., 2021). Hence, the most up-dip occurrence of fluvial channel fill deposits representative for backwater conditions might be related to deposition contemporaneous to a younger shoreline. Backwater calculations in low-accommodation settings may not capture the full evolution of backwater influence.

5.4. Importance of backwater length accuracy and future work

Backwater length estimates are commonly used to assess scaling

relationships with avulsion lengths (Jerolmack, 2009; Chatanantavet et al., 2012; Ganti et al., 2014, 2016; Hartley et al., 2016; Brooke et al., 2020; Prasojo et al., 2021; Brooke et al., 2021), relationship with changes in sedimentary trends and channel morphology (Nittrouer et al., 2011, 2012; Fernandes et al., 2016; Gugliotta et al., 2017; Smith et al., 2020; Hassenruck-Gudipati et al., 2022), and changes in preserved fluvial strata (Colombera et al., 2016; Lin and Bhattacharya, 2017; Milliken et al., 2018; Martin et al., 2018; Trower et al., 2018; Lin et al., 2020; van Yperen et al., 2021). The strength of these relations is determined by backwater length accuracy. If there is a strong correlation between backwater length, avulsion scale and changes in sedimentary trends, then the backwater length becomes a useful predictor of these other changes, and thus accurate estimation of backwater length becomes important as a predictor of related changes in fluvial architecture. If the relationship is weak, the accuracy becomes less relevant.

Additionally, there is ongoing investigation on potential geometric scaling (i.e. without need for flood discharge variability; Chadwick et al., 2019; Ratliff et al., 2021), valley exit control (Hartley et al., 2016), bedslope changes (Prasojo et al., 2021), and backwater-scaled avulsions (e.g. Ganti et al., 2016; Brooke et al., 2021). Considering results that support the latter, scaling between the avulsion length and backwater length approximate a near 1:1 relationship when considering only the deltas with backwater-scaled avulsions (Brooke et al., 2021). More precisely however, their result La* = La/Lb is 0.87 ± 0.38, (La* is dimensionless avulsion length, La is avulsion length, Lb is backwater length) implies that a backwater length estimate of 300 km could relate to an avulsion node between 147 and 375 km, in addition to 37.5% of the 80 analyzed delta-plain avulsions not having a backwater-scaled avulsion. The backwater length estimates in Brooke et al. (2021) are partly based on slope and channel depth estimates that were previously published, which we demonstrated are obtained in numerous ways.

Future work in modern river systems should further investigate the differences between backwater length estimates resulting from direct riverbed surveys combined with water elevation profiles versus backwater length estimates based on indirectly obtained parameters and the h/S approach, and eventually assess their relation to changes in channel morphology and sedimentary trends. In ancient settings, a potential link between dimensionless updip backwater transition zone and outcrop evidences for changing fluvial architectural style should be further exploited.

6. Conclusions

- Backwater length estimates for the same river system may vary up to a factor 10, due to the use of different methods and equivocal sources and definitions of the input parameters channel depth and slope.
- The lack of standardized methodology hinders comparability and applicability of previously established and future backwater length estimates, and their corresponding influence on the hydrodynamic environment and ultimately the stratigraphic record.
- Identification of river bed intersection with sea level is best for backwater length estimates in modern settings. Indirectly derived backwater length estimates (Lb = h/S) are most accurate when bankfull thalweg channel depth is obtained from a cross-sectional profile. We recommend avoiding the use of discharge and grain size to obtain bankfull thalweg channel depth as resulting backwater length estimates plot into the non-uniform flow reach, which is the backwater zone itself.
- Backwater length estimates in ancient settings are most accurate when derived from intact channel story thickness and empirically estimated slope using grain size. Testing on an ancient case study demonstrates these estimates align with changes in outcrop fluvial architectural style.
- A discrete backwater-length value is rarely applicable for an ancient stratigraphic unit, but is rather best represented by a range of mean and standard deviation from some broader sampling of a representative collection of channel stories in the layer.
- Despite uncertainties the backwater concept holds potential in predictability of change in channel morphology and architectural style in both modern and ancient settings, and has major potential for subsurface exploration, aquifer management and geohazards.

Acknowledgements

This manuscript benefited from discussions with Massimiliano Ghinassi, Alvise Finotello and Valentin Zuchuat. Cody Myers is thanked for grain size analysis. The study was funded by AkerBP. We thank two anonymous reviewers for their constructive comments, as well as editor Christopher Fielding and guest editor Julien Bailleul.

Declaration of competing interest

The authors declare that they have no known competing financial interests or personal relationships that could have appeared to influence the work reported in this paper.

Data availability

The data that support the findings of this study are available from the corresponding author upon reasonable request.

Appendix A. Supplementary data

Supplementary data to this article can be found online at https://doi.org/10.1016/j.earscirev.2024.104692.

References

Allen, J.R.L., 1982. Empirical character of ripples and dunes formed by unidirectional flows. In: L.Allen, J.R. (Ed.), Sedimentary structures: Their character and physical basis, developments in sedimentology. Elsevier, Amsterdam, pp. 307–344.

Allen, J.R.L., 1983. Studies in fluviatile sedimentation: bars, bar-complexes and sandstone sheets (low-sinuosity braided streams) in the Brownstones (L. Devonian), Welsh Borders. Sediment. Geol. 33 (4), 237–293. https://doi.org/10.1016/0037-0738(83)90076-3.

Allen, J.R.L., 1986. The nature and origin of bed-form hierarchies. Sedimentology 10 (3), 161–182.

Amarnath, C.R., Thatikonda, S., 2020. Study on backwater effect due to Polavaram Dam Project under different return periods. Water 12 (2), 576. https://doi.org/10.3390/W12020576.

Beck, H.E., Zimmermann, N.E., McVicar, T.R., Vergopolan, N., Berg, A., Wood, E.F., 2018. Present and future Köppen-Geiger climate classification maps at 1-km resolution. Scientific data 5 (1), 1–12. https://doi.org/10.1038/sdata.2018.214.

Best, J.L., Ashworth, P.J., 1997. Scour in large braided rivers and the recognition of sequence stratigraphic boundaries. Nature 387 (6630), 275–277.

Best, J., Fielding, C.R., 2019. Describing fluvial systems: Linking processes to deposits and stratigraphy. Geol. Soc. London, Spec. Pub. 488, 152–166. https://doi.org/10.1144/SP488-2019-056.

Bhattacharya, J.P., Copeland, P., Lawton, T.F., Holbrook, J.M., 2016. Estimation of source area, river paleo-discharge, paleoslope, and sediment budgets of linked deep-time depositional systems and implications for hydrocarbon potential. Earth Sci. Rev. 153, 77–110. https://doi.org/10.1016/j.earscirev.2015.10.013.

Bjerklie, D.M., Birkett, C.M., Jones, J.W., Carabajal, C., Rover, J.A., Fulton, J.W., Garambois, P.A., 2018. Satellite remote sensing estimation of river discharge: application to the Yukon River Alaska. J. Hydrol. 561, 1000–1018. https://doi.org/10.1016/j.jhydrol.2018.04.005.

Blum, M., Martin, J., Milliken, K., Garvin, M., 2013. Paleovalley systems: Insights from Quaternary analogs and experiments. Earth Sci. Rev. 116 (1), 128–169. https://doi.org/10.1016/j.earscirev.2012.09.003.

Bradley, R.W., Venditti, J.G., 2017. Reevaluating dune scaling relations. Earth Sci. Rev. 165, 356–376. https://doi.org/10.1016/j.earscirev.2016.11.004.

Bridge, J.S., 2003. Rivers and Floodplains. Blackwell Scientific Publications, Oxford, U.K.

Bridge, J.S., Mackey, S.D., 1993. A revised alluvial stratigraphy model. In: Marzo, M., Puigdefabregas, C. (Eds.), Alluvial Sedimentation. International Association of Sedimentologists, pp. 319–336. Special Publication 17.

Bridge, J.S., Tye, R.S., 2000. Interpreting the dimensions of ancient fluvial channel bars, channels, and channel belts from wireline-logs and cores. AAPG Bull. 84 (8), 1205–1228. https://doi.org/10.1306/A9673C84-1738-11D7-8645000102C1865D.

Bridge, J.S., Jalfin, G.A., Georgieff, S.M., 2000. Geometry, lithofacies, and spatial distribution of cretaceous fluvial sandstone bodies, San Jorge Basin, Argentina:

outcrop analog for the hydrocarbon-bearing Chubut Group. J. Sediment. Res. 70 (2), 341–359. https://doi.org/10.1306/2DC40915-0E47-11D7-8643000102C1865D.
Brooke, S., Ganti, V., Chadwick, A.J., Lamb, M.P., 2020. Flood variability determines the location of lobe-scale avulsions on deltas: Madagascar. Geophys. Res. Lett. 47 (20) https://doi.org/10.1029/2020GL088797.
Brooke, S., Chadwick, A.J., Silvestre, J., Lamb, M.P., Edmonds, D.A., Ganti, V., 2022. Where rivers jump course. Science 376 (6596), 987–990. https://doi.org/10.1126/science.abm1215.
Brooks, H.L., Steel, E., Moore, M., 2022. Grain-size analysis of ancient deep-marine sediments using laser diffraction. Front. Earth Sci. 10 (564) https://doi.org/10.3389/feart.2022.820866.
Carey, W.C., Keller, M.D., 1957. Systematic changes in the beds of alluvial rivers. J. Hydraul. Div. 83 (4), 1331.
Chadwick, A.J., Lamb, M.P., Moodie, A.J., Parker, G., Nittrouer, J.A., 2019. Origin of a preferential avulsion node on lowland river deltas. Geophys. Res. Lett. 46 (8), 4267–4277. https://doi.org/10.1029/2019GL082491.
Chatanantavet, P., Lamb, M.P., 2014. Sediment transport and topographic evolution of a coupled river and river plume system: an experimental and numerical study. J. Geophys. Res. Earth 119, 1263–1282. https://doi.org/10.1002/2013JF002810.
Chatanantavet, P., Lamb, M.P., Nittrouer, J.A., 2012. Backwater controls of avulsion location on deltas. Geophys. Res. Lett. 39 (1) https://doi.org/10.1029/2011GL050197.
Chow, V.T., 1959. Open-Channel Hydraulics. McGraw-Hill, New York.
Cohen, S., Kettner, A.J., Syvitski, J.P.M., 2014. Global suspended sediment and water discharge dynamics between 1960 and 2010: Continental trends and intra-basin sensitivity. Global Planet. Change 115, 44–58. https://doi.org/10.1016/j.gloplacha.2014.01.011.
Colombera, L., Shiers, M.N., Mountney, N.P., 2016. Assessment of backwater controls on the architecture of distributary-channel fills in a tide-influenced coastal-plain succession: Campanian Neslen Formation, U.S.A. J. Sediment. Res. 86 (5), 476–497. https://doi.org/10.2110/jsr.2016.33.
Csiki, S., Rhoads, B.L., 2010. Hydraulic and geomorphological effects of run-of-river dams. Progr. Physical Geogr. Earth Environ. 34 (6) https://doi.org/10.1177/0309133310369435.
Dunne, K.B., Jerolmack, D.J., 2018. Evidence of, and a proposed explanation for, bimodal transport states in alluvial rivers. Earth Surface Dynamics 6 (3), 583–594. https://doi.org/10.5194/esurf-6-583-2018.
Fernandes, A.M., Törnqvist, T.E., Straub, K.M., Mohrig, D., 2016. Connecting the backwater hydraulics of coastal rivers to fluvio-deltaic sedimentology and stratigraphy. Geology 44 (12), 979–982. https://doi.org/10.1130/G37965.1.
Fielding, C.R., Crane, R.C., 1987. An application of statistical modelling to the prediction of hydrocarbon recovery factors in fluvial reservoir sequences. In: Ethridge, F.G., Flores, R.M., Harvey, M.D. (Eds.), Recent Developments in Fluvial Sedimentology, pp. 321–327. SEPM Special Publication 39.
Ganti, V., Chu, Z., Lamb, M.P., Nittrouer, J.A., Parker, G., 2014. Testing morphodynamic controls on the location and frequency of river avulsions on fans versus deltas: Huanghe (Yellow River), China. Geophys. Res. Lett. 41, 7882–7890. https://doi.org/10.1002/2014GL061918.
Ganti, V., Chadwick, A.J., Hassenruck-Gudipati, H.J., Fuller, B.M., Lamb, M.P., 2016. Experimental river delta size set by multiple floods and backwater hydrodynamics. Sci. Adv. 2 (5), e1501768 https://doi.org/10.1126/sciadv.1501768.
Ganti, V., Lamb, M.P., Chadwick, A.J., 2019. Autogenic erosional surfaces in fluvio-deltaic stratigraphy from floods, avulsions, and backwater hydrodynamics. J. Sediment. Res. 89 (9), 815–832. https://doi.org/10.2110/jsr.2019.40.
Ghosh, P., 2000. Estimation of channel sinuosity from paleocurrent data: a method using fractal geometry. J. Sediment. Res. 70 (3), 449–455. https://doi.org/10.1306/2DC4091D-0E47-11D7-8643000102C1865D.
Gibling, M.R., 2006. Width and thickness of fluvial channel bodies and valley fills in the geological record: a literature compilation and classification. J. Sediment. Res. 76 (5), 731–770. https://doi.org/10.2110/jsr.2006.060.
Gingerich, P.D., 2019. Temporal scaling of carbon emission and accumulation rates: modern anthropogenic emissions compared to estimates of PETM onset accumulation. Paleoceanogr. Paleoclimatol. 34 (3), 329–335. https://doi.org/10.1029/2018PA003379.
Graf, W.L., 1988. Fluvial Processes in Dryland Rivers, 1st ed. Springer-Verlag https://link.springer.com/book/9783540175919.
Gugliotta, M., Saito, Y., 2019. Matching trends in channel width, sinuosity, and depth along the fluvial to marine transition zone of tide-dominated river deltas: the need for a revision of depositional and hydraulic models. Earth Sci. Rev. 191, 93–113. https://doi.org/10.1016/J.EARSCIREV.2019.02.002.
Gugliotta, M., Saito, Y., Nguyen, V.L., Ta, T.K.O., Nakashima, R., Tamura, T., Uehara, K., Katsuki, K., Yamamoto, S., 2017. Process regime, salinity, morphological, and sedimentary trends along the fluvial to marine transition zone of the mixed-energy Mekong River delta, Vietnam. Cont. Shelf Res. 147, 7–26. https://doi.org/10.1016/J.CSR.2017.03.001.
Hajek, E.A., Heller, P.L., 2012. Flow-depth scaling in alluvial architecture and nonmarine sequence stratigraphy: example from the Castlegate Sandstone, Central Utah, U.S.a. J. Sediment. Res. 82 (2), 121–130. https://doi.org/10.2110/JSR.2012.8.
Hajek, E.A., Wolinsky, M.A., 2012. Simplified process modeling of river avulsion and alluvial architecture: Connecting models and field data. Sediment. Geol. 257, 1–30. https://doi.org/10.1016/J.SEDGEO.2011.09.005.
Hansford, M.R., Plink-Björklund, P., Jones, E.R., 2020. Global quantitative analyses of river discharge variability and hydrograph shape with respect to climate types. Earth Sci. Rev. 200 (102977) https://doi.org/10.1016/j.earscirev.2019.102977.
Harmar, O.P., Clifford, N.J., 2007. Geomorphological explanation of the long profile of the Lower Mississippi River. Geomorphology 84 (3–4), 222–240. https://doi.org/10.1016/j.geomorph.2006.01.045.
Hartley, A.J., Owen, A., 2022. Paleohydraulic analysis of an ancient distributive fluvial system. J. Sediment. Res. 92, 445–459. https://doi.org/10.2110/jsr.2021.062.
Hartley, A.J., Weissmann, G.S., Scuderi, L., 2016. Controls on the apex location of large deltas. J. Geol. Soc. Lond. 174 (1), 10–13. https://doi.org/10.1144/jgs2015-154.
Hassenruck-Gudipati, H.J., Passalacqua, P., Mohrig, D., 2022. Natural levees increase in prevalence in the backwater zone: Coastal Trinity River, Texas, USA. Geology 50 (9), 1068–1072. https://doi.org/10.1130/G50011.1.
Holbrook, J.M., 1996. Complex fluvial response to low gradients at maximum regression; a genetic link between smooth sequence-boundary morphology and architecture of overlying sheet sandstone. J. Sediment. Res. 66 (4), 713–722. https://doi.org/10.1306/D42683EC-2B26-11D7-8648000102C1865D.
Holbrook, J.M., 2001. Origin, genetic interrelationships, and stratigraphy over the continuum of fluvial channel-form bounding surfaces: an illustration from middle Cretaceous strata, Southeastern Colorado. Sediment. Geol. 144 (3–4), 179–222. https://doi.org/10.1016/S0037-0738(01)00118-X.
Holbrook, J.M., Miall, A.D., 2020. Time in the Rock: a field guide to interpreting past events and processes from siliciclastic stratigraphy. Earth Sci. Rev. 203, 103121 https://doi.org/10.1016/j.earscirev.2020.103121.
Holbrook, J.M., Wanas, H., 2014. A fulcrum approach to assessing source-to-sink mass balance using channel paleohydrologic paramaters derivable from common fluvial data sets with an example from the cretaceous of Egypt. J. Sediment. Res. 84 (5), 349–372. https://doi.org/10.2110/jsr.2014.29.
Holbrook, J.M., Scott, R.W., Oboh-Ikuenobe, F.E., 2006. Base-level buffers and buttresses: a model for upstream versus downstream control on fluvial geometry and architecture within sequences. J. Sediment. Res. 76 (1), 162–174. https://doi.org/10.2110/jsr.2005.10.
Hudson, P.F., Kesel, R.H., 2000. Channel migration and meander-bend curvature in the lower Mississippi River prior to major human modification. Geology 28 (6), 531–534. https://doi.org/10.1130/0091-7613(2000)28<531:CMAMCI>2.0.CO;2.
Jerolmack, D.J., 2009. Conceptual framework for assessing the response of delta channel networks to Holocene Sea level rise. Quat. Sci. Rev. 28 (17–18), 1786–1800. https://doi.org/10.1016/J.QUASCIREV.2009.02.015.
Jerolmack, D.J., Mohrig, D., 2007. Conditions for branching in depositional rivers. Geology 35 (5), 463–466. https://doi.org/10.1130/G23308A.1.
Kimmerle, S., Bhattacharya, J.P., 2018. Facies, backwater limits, and paleohydraulic analysis of rivers in a forced-regressive, compound incised valley, Cretaceous Ferron Sandstone, Utah, U.S.A. J. Sediment. Res. 88, 177–200. https://doi.org/10.2110/jsr.2018.5.
Lamb, M.P., Nittrouer, J.A., Mohrig, D., Shaw, J., 2012. Backwater and river plume controls on scour upstream of river mouths: implications for fluvio-deltaic morphodynamics. J. Geophys. Res. 117, F01002. https://doi.org/10.1029/2011JF002079.
Le Roux, J.P., 1992. Determining the channel sinuosity of ancient fluvial systems from paleocurrent data. J. Sediment. Res. 62 (2), 283–291. https://doi.org/10.1306/D42678E3-2B26-11D7-8648000102C1865D.
Le Roux, J.P., 1994. The angular deviation of paleocurrent directions as applied to the calculation of channel sinuosities. J. Sediment. Res. 64 (1), 86–87.
Leclair, S.F., Bridge, J.S., 2001. Quantitative interpretation of sedimentary structures formed by river dunes. J. Sediment. Res. 71 (5), 713–716. https://doi.org/10.1306/2DC40962-0E47-11D7-8643000102C1865D.
Leeder, M.R., 1973. Fluviatile fining-upwards cycles and the magnitude of palaeochannels. Geol. Mag. 110, 265–276.
Lin, W., Bhattacharya, J.P., 2017. Estimation of source-to-sink mass balance by a fulcrum approach using channel paleohydrologic parameters of the Cretaceous Dunvegan Formation, Canada. J. Sediment. Res. 87 (1), 97–116. https://doi.org/10.2110/jsr.2017.1.
Lin, W., Ferron, C., Karner, S., Bhattacharya, J.P., 2020. Classification of paralic channel sub-environments in an ancient system using outcrops: the Cretaceous Gallup system, New Mexico, U.S.a. J. Sediment. Res. 90 (9), 1094–1113. https://doi.org/10.2110/JSR.2019.191.
Liro, M., 2019. Dam reservoir backwater as a field-scale laboratory of human-induced changes in river biogeomorphology: a review focused on gravel-bed rivers. Sci. Total Environ. 651, 2899–2912. https://doi.org/10.1016/J.SCITOTENV.2018.10.138.
Liro, M., Ruiz-Villanueva, V., Mikuś, P., Wyżga, B., Bladé Castellet, E., 2020. Changes in the hydrodynamics of a mountain river induced by dam reservoir backwater. Sci. Total Environ. 744 (140555) https://doi.org/10.1016/J.SCITOTENV.2020.140555.
Long, D.G.F., 2021. Trickling down the paleoslope: an empirical approach to paleohydrology. Earth Sci. Rev. 220, 103740 https://doi.org/10.1016/J.EARSCIREV.2021.103740.
Lynds, R., Mohrig, D., Hajek, E.A., Heller, P.L., 2014. Paleoslope reconstruction in sandy suspended-load-dominant rivers. J. Sediment. Res. 84, 825–836. https://doi.org/10.2110/jsr.2014.60.
Lyster, S.J., Whittaker, A.C., Hampson, G.J., Hajek, E.A., Allison, P.A., Lathrop, B.A., 2021. Reconstructing the morphologies and hydrodynamics of ancient rivers from source to sink: Cretaceous Western Interior Basin, Utah, USA. Sedimentology 68 (6), 2854–2886. https://doi.org/10.1111/sed.12877.
Lyster, S.J., Whittaker, A.C., Farnsworth, A., Hampson, G.J., 2023. Constraining flow and sediment transport intermittency in the geological past. GSA Bull. https://doi.org/10.1130/B36873.1.
Mackin, J.H., 1948. Concept of the graded river. Geol. Soc. Am. Bull. 59 (5), 463–512.
Martin, J., Fernandes, A.M., Pickering, J., Howes, N., Mann, S., McNeil, K., 2018. The stratigraphically preserved signature of persistent backwater dynamics in a large

paleodelta system: the Mungaroo Formation, North West Shelf, Australia. J. Sediment. Res. 88 (7), 850–872. https://doi.org/10.2110/jsr.2018.38.
Maselli, V., Pellegrini, C., Del Bianco, F., Mercorella, A., Nones, M., Crose, L., Guerrero, M., Nittrouer, J.A., 2018. River morphodynamic evolution under dam-induced backwater: an example from the Po River (Italy). J. Sediment. Res. 88 (10), 1190–1204. https://doi.org/10.2110/JSR.2018.61.
Mclaurin, B.T., Steel, R.J., 2007. Architecture and origin of an amalgamated fluvial sheet sand, lower Castlegate Formation, Book Cliffs, Utah. Sediment. Geol. 197, 291–311. https://doi.org/10.1016/j.sedgeo.2006.10.005.
Milliken, K.T., Blum, M.D., Snedden, J.W., Galloway, W.E., 2018. Application of fluvial scaling relationships to reconstruct drainage-basin evolution and sediment routing for the cretaceous and Paleocene of the Gulf of Mexico. Geosphere 14 (2), 749–767. https://doi.org/10.1130/GES01374.1.
Molnar, P., Anderson, R.S., Kier, G., Rose, J., 2006. Relationships among probability distributions of stream discharges in floods, climate, bed load transport, and river incision. J. Geophys. Res. Earth 111 (F2). https://doi.org/10.1029/2005JF000310.
Nittrouer, J.A., 2013. Backwater hydrodynamics and sediment transport in the lowermost Mississippi River Delta: Implications for the development of fluvial-deltaic landforms in a large lowland river. *Deltas: Landforms, Ecosystems, and Human Activities: International Association of Hydrological Sciences Publication*, pp. 48–61.
Nittrouer, J.A., Mohrig, D., Allison, M., 2011. Punctuated sand transport in the lowermost Mississippi River. J. Geophys. Res. Earth 116 (F4), 4025. https://doi.org/10.1029/2011JF002026.
Nittrouer, J.A., Lamb, M.P., Mohrig, D., 2012. Spatial and temporal trends for water-flow velocity and bed-material sediment transport in the lower Mississippi River. Geol. Soc. Am. Bull. 124 (3–4), 400–414. https://doi.org/10.1130/B30497.1.
Oboh-Ikuenobe, F.E., Holbrook, J.M., Scott, R.W., Akins, S.L., Evetts, M.J., Benson, D.G., Pratt, L.M., 2008. Anatomy of epicontinental flooding: Late Albian-Early Cenomanian of the southern U.S. Western Interior Basin. In: Pratt, B.R., Holmden, C. (Eds.), Dynamics of Epeiric Seas, vol. Issue 48. Geological Association of Canada, Special Paper, pp. 201–227. https://doi.org/10.1016/0016-7037(86)90064-5.
Paola, C., Borgman, L., 1991. Reconstructing random topography from preserved stratification. Sedimentology 38 (4), 553–565. https://doi.org/10.1111/j.1365-3091.1991.tb01008.x.
Paola, C., Mohrig, D., 1996. Palaeohydraulics revisited: palaeoslope estimation in coarse-grained braided rivers. Basin Res. 8 (3), 243–254. https://doi.org/10.1046/J.1365-2117.1996.00253.X.
Paola, C., Parker, G., Seal, R., Sinha, S.K., Southard, J.B., Wilcock, P.R., 1992. Downstream fining by selective deposition in a laboratory flume. Science 258 (5089), 1757–1760. https://doi.org/10.1126/science.258.5089.1757.
Parker, G., 1978. Self-formed straight rivers with equilibrium banks and mobile bed. Part 2. The gravel river. J. Fluid Mech. 89 (1), 127–146.
Parker, G., Wilcock, P.R., Paola, C., Dietrich, W.E., Pitlick, J., 2007. Physical basis for quasi-universal relations describing bankfull hydraulic geometry of single-thread gravel bed rivers. J. Geophys. Res. Earth 112 (F4), 4005. https://doi.org/10.1029/2006JF000549.
Phillips, J.D., Slattery, M.C., Musselman, Z.A., 2005. Channel adjustments of the lower Trinity River, Texas, downstream of Livingston Dam. Earth Surface Processes and Landforms: The Journal of the British Geomorphological Research Group 30 (11), 1419–1439. https://doi.org/10.1002/esp.1203.
Pickup, G., Rieger, W.A., 1979. A conceptual model of the relationship between channel characteristics and discharge. Earth Surface Processes 4 (1), 37–42. https://doi.org/10.1002/ESP.3290040104.
Pickup, G., Warner, R.F., 1976. Effects of hydrologic regime on magnitude and frequency of dominant discharge. J. Hydrol. 29 (1–2), 51–75. https://doi.org/10.1016/0022-1694(76)90005-6.
Prasojo, O.A., Hoey, T.B., Owen, A., Williams, R.D., 2021. Slope break and avulsion locations scale consistently in global deltas. Geophys. Res. Lett. 49 (2) https://doi.org/10.1029/2021GL093656 e2021GL093656.
Ratliff, K.M., Hutton, E.W.H., Murray, A.B., 2021. Modeling long-term delta dynamics reveals persistent geometric river avulsion locations. Earth Planet. Sci. Lett. 559, 116786 https://doi.org/10.1016/J.EPSL.2021.116786.
Rittenour, T.M., Blum, M.D., Goble, R.J., 2007. Fluvial evolution of the lower Mississippi River valley during the last 100 k.y. glacial cycle: response to glaciation and sea-level change. GSA Bull. 119 (5–6), 586–608. https://doi.org/10.1130/B25934.1.
Rubin, D.M., Carter, C.L., 1987. Cross-bedding, bedforms, and paleocurrents, 1, 187-undefined.
Scott, R.W., Holbrook, J.M., Oboh-Ikuenobe, F.E., Evetts, M.J., Benson, D.G., Kues, B.S., 2004. Middle Cretaceous stratigraphy, southern Western Interior Seaway, New Mexico and Oklahoma. Rocky Mountain Assoc. Geol. 41 (2), 33–61.
Shields, A., 1936. Anwendung der Ähnlichkeitsmechanik und der Turbulenzforschung auf die Geschiebebewegung [Application of Similarity Principles and Turbulence Research to Bed-Load Movement]. Preußische Versuchsanstalt Für Wasserbau Und Schiffbau 26, 47.
Shiers, M.N., Mountney, N.P., Hodgson, D.M., Colombera, L., 2018. Controls on the depositional architecture of fluvial point-bar elements in a coastal-plain succession. Fluvial Meanders and Their Sedimentary Products in the Rock Record 15–46. https://doi.org/10.1002/9781119424437.CH2.
Smith, V., Mason, J., Mohrig, D., 2020. Reach-scale changes in channel geometry and dynamics due to the coastal backwater effect: the lower Trinity River, Texas. Earth Surf. Process. Landf. 45 (3), 565–573. https://doi.org/10.1002/ESP.4754.
Surian, N., Mao, L., Giacomin, M., Ziliani, L., 2009. Morphological effects of different channel-forming discharges in a gravel-bed river. Earth Surf. Process. Landf. 34 (8), 1093–1107. https://doi.org/10.1002/ESP.1798.
Trampush, S.M., Huzurbazar, S., McElroy, B., 2014. Empirical assessment of theory for bankfull characteristics of alluvial channels. Water Resour. Res. 50, 9211–9220. https://doi.org/10.1002/2014WR015597.
Trower, E.J., Ganti, V., Fischer, W.W., Lamb, M.P., 2018. Erosional surfaces in the Upper cretaceous Castlegate Sandstone (Utah, USA): Sequence boundaries or autogenic scour from backwater hydrodynamics? Geology 46 (8), 707–710. https://doi.org/10.1130/G40273.1.
USACE, 1935. Studies of river bed materials and their movement, with special reference to the lower Mississippi River. In: US Army Corps Engineers, US Waterways Experiment Station, Vicksburg, Mississippi, Paper, 17, 161 p.
Van Yperen, A.E., Holbrook, J.M., Poyatos-Moré, M., Midtkandal, I., 2019. Coalesced delta-front sheet-like sandstone bodies from highly avulsive distributary channels: the low-accommodation Mesa Rica Sandstone (Dakota Group, New Mexico, U.S.A.). J. Sediment. Res. 89 (7), 654–678. https://doi.org/10.2110/jsr.2019.27.
van Yperen, A.E., Holbrook, J.M., Poyatos-Moré, M., Myers, C., Midtkandal, I., 2021. Low-accommodation and backwater effects on sequence stratigraphic surfaces and depositional architecture of fluvio-deltaic settings (Cretaceous Mesa Rica Sandstone, Dakota Group, USA). Basin Res. 33 (1), 513–543. https://doi.org/10.1111/bre.12483.
Venditti, J.G., 2013. 9.10 bedforms in sand-bedded rivers. Treatise on geomorphology 9, 137–162.
Williams, G.P., 1978. Bankfull discharge of rivers. Water Resour. Res. 1 (14), 1141–1158.
Wright, S., Parker, G., 2005. Modeling downstream fining in sand-bed rivers. I: Formulation. J. Hydraul. Res. 43 (6), 613–620. https://doi.org/10.1080/00221680509500381.
Wu, C., Nittrouer, J.A., Barefoot, E.A., Burmeister, K.C., 2023. Reconstructing backwater hydrodynamics from fluvial-deltaic deposits using stratigraphic inversion: an example from the Tullig Sandstone, Western Irish Namurian Basin, County Clare, Ireland. GSA Bull. 135 (9–10), 2315–2330. https://doi.org/10.1130/B36475.1.
Yalin, M.S., 1964. Geometrical properties of sand wave. J. Hydraulics Div. 90 (5), 105–119. https://doi.org/10.1061/JYCEAJ.0001097.
Yamazaki, D., Kanae, S., Kim, H., Oki, T., 2011. A physically based description of floodplain inundation dynamics in a global river routing model. Water Resour. Res. 47, 2010WR009726 10.1029/2010WR009726.
Zhu, Y., Bhattacharya, J.P., Li, W., Lapen, T.J., Jicha, B.R., Singer, B.S, 2012. Milankovitch-scale sequence stratigraphy and stepped forced regressions of the Turonian Ferron Notom deltaic complex, south-central Utah, USA. J. Sediment. Res. 82 (9), 723–746. https://doi.org/10.2110/jsr.2012.63.